JOURNAL OF GEOPHYSICAL RESEARCH, VOL. 95, NO. C7, PAGES 11,501–11,530, JULY 15, 1990

Seasonal and Nonseasonal Variability of Satellite-Derived Surface Pigment Concentration in the California Current

P. Ted Strub, Corinne James, Andrew C. Thomas, and Mark R. Abbott

College of Oceanography, Oregon State University, Corvallis

Satellite-derived pigment concentrations from the west coast time series (WCTS) are averaged into monthly mean fields over the California Current system (CCS) for the period July 1979 to June 1986. Errors caused by the scattering algorithm used in the WCTS are reduced by an empirical correction function, although winter values (November–February) remain unreliable. For the March–October period we look at both the mean seasonal development and the nonseasonal monthly anomalies of pigment concentration. These are compared with fields of alongshore wind stress, mixing power of the wind (u_*^3) and wind stress curl. Outside of the Southern California Bight there is a strong seasonal cycle with a spring–summer maximum, a northward progression of high pigment concentrations from California to Oregon and a double maximum off Washington (spring and summer, with a lull in between). Within the Southern California Bight, seasonality is low, with a relative minimum in late summer. Off Baja California the pattern is similar to that off northern California. In regions where previous work has been done, there is general agreement with the seasonal cycles found here. Nonseasonal variability in pigment concentration over the large-scale CCS (400 km wide) is most closely related statistically to synoptic fields of wind stress curl. Within 100 km of the coast, the strongest relations are between pigment concentration and both u_*^3 and alongshore wind stress. Correlations with these wind variables account for only 25% of the monthly variance in anomalous satellite-derived pigment concentrations. This is partly due to the noise in both wind and pigment data sets but also demonstrates the fact that much of the anomalous pigment variability is not a response to anomalous wind forcing on these time scales. Correlations are also low between anomalous pigment concentrations and anomalous sea level heights, which serve as a crude proxy for the strength of the alongshore current over the shelf. The largest nonseasonal anomaly in the data occurred during the 1982–1983 El Niño, which caused a large-scale decrease in pigment concentration, stronger and longer lasting in the south than in the north.

1. Introduction

The large-scale patterns of satellite-derived surface pigment concentration off the west coast of North America are presented and their statistical relation to surface wind forcing are examined. Spatial patterns in the California Current system (CCS) between approximately 25°N and 50°N, and between 105°W and 140°W are discussed in terms of both seasonal and nonseasonal variability over the period July 1979 to June 1986.

Although previous studies have utilized satellite data from the coastal zone color scanner (CZCS) to show spatial and temporal patterns of surface pigment concentration within the CCS, most have treated restricted time periods and/or relatively small spatial regions [*Abbott and Zion*, 1985, 1987; *Barale and Fay*, 1986; *Peláez and McGowan*, 1986; *Michaelsen et al.*, 1988; *Smith et al.*, 1988]. Our approach is to examine the large-scale variability by averaging data into monthly means within 1° spatial blocks. Although this temporal and spatial averaging eliminates much of the mesoscale variability that has been the focus of the CZCS analyses cited above [*Denman and Abbott*, 1988], it does produce a more regular time series than that provided by the temporally and spatially patchy individual images and makes quantitative use of the entire west coast time series (WCTS) of CZCS data.

The satellite time series provides a unique opportunity to test connections between wind forcing and biological response in the upper ocean over a seven year period in an eastern boundary current system. An increasing number of studies have looked for correlations between monthly (or shorter) averages of alongshore wind stress (as an upwelling index) and indicators of biological productivity at higher trophic levels [*Bakun*, 1973; *Botsford*, 1986; *Botsford et al.*, 1989; *Landry et al.*, 1989]. It is therefore appropriate to test the connection between wind forcing and pigment concentration, a variable approximating the time integral of previous primary productivity in the upper ocean.

In section 2 we summarize the large-scale seasonal characteristics of the California Current; this section can be skipped by those familiar with this region. Section 3 describes the data and methods used here and discusses problems known to affect the satellite-derived pigment concentrations and the wind data used in this study. In section 4 we present the results of the statistical analysis, and in section 5 these results are discussed in light of past observations and theory. Section 6 summarizes the main conclusions of the study with reference to the pertinent figures. Sections 3–6 are divided into subsections which consider the seasonal and nonseasonal variability separately. Appendix A describes details of the CZCS data processing. Appendix B gives the details of the principal estimator pattern methodology.

Paper number 89JC03739.
0148-0227/90/89JC-03739$05.00

2. The California Current System

The CCS is the equatorward eastern boundary current (EBC) of the North Pacific, connecting the eastward flowing west wind drift in the north (approximately 45°–50°N) to the westward flowing North Equatorial Current in the south (approximately 20°N). The CCS has a fairly regular geometry and narrow shelf. Previous work has shown regional differences in both the physical and biological oceanography within the CCS. Although no single work provides a detailed comparison of regions within the CCS, the literature suggests differences in the forcing and response between the Washington–Oregon coasts, the northern–central California coasts, the Southern California Bight, and the Baja California coast.

2.1. *Physical Overview*

Water entering the CCS from the north is relatively cold, fresh and rich in nutrients. Water to the west of the current is warmer and lower in nutrients. In the south and away from the coast off Baja California, water is warm, salty and low in nutrients [*Hickey*, 1979; *Freeland et al.*, 1984; *Martin and Gordon*, 1988; *Scripps Institution of Oceanography*, 1984*a*, 1984*b*, 1984*c*, 1984*d*]. During spring and summer upwelling, water close to the coast is cold, salty, and high in nutrients, except where it is influenced by the fresh water from rivers such as the Fraser and Columbia and from San Francisco Bay [*Huyer*, 1983; *Traganza et al.*, 1983]. North of ≈ 34°N, shelf regions experience episodic upwelling events even in winter; in the southern portions of the CCS, winds are upwelling favorable throughout the year [*Strub et al.*, 1987*a*]. Coastal upwelling, increased mixing over the shelf and topographic effects combine to produce a nearshore band of higher nutrient levels and pigment concentrations all year [*Barale and Fay*, 1986].

The climatological picture of the CCS current regime in summer consists of southward meandering surface flow, with a maximum velocity over the shelf off Oregon and Washington, ≈ 150 km offshore off central California and close to the coast again off Baja California. Off southern California (≈ 32°N) the current has a strong onshore component and flows eastward. Part of this flow turns south along the Baja California coast and part flows northward into the Southern California Bight [*Pavlova*, 1966; *Hickey*, 1979, 1989; *Pares-Sierra and O'Brien*, 1989; *Niiler et al.*, 1989]. The historical hydrographic data [*Hickey*, 1979; *Roesler and Chelton*, 1987] and the model of *Pares-Sierra and O'Brien* [1989] suggest that the flow into the bight is strongest in summer. Within the bight itself, the circulation often consists of a cyclonic gyre. In winter, southward flow is weaker and farther offshore, and the northward flowing Davidson Current is found next to the coast [*Hickey*, 1979].

Off central Oregon and Washington, alongshore currents over the shelf are quite regular, flowing southward for most of the spring and summer and fluctuating with storm winds in fall and winter [*Huyer et al.*, 1979]. The Columbia River plume is advected to the south in summer, influencing the coast of Oregon, and to the north in winter, influencing the coast of Washington [*Hickey*, 1989]. Between Cape Blanco and Point Conception (43°–35°N) the currents over the shelf exhibit large fluctuations with periods of 20–40 days [*Strub et al.*, 1987*a*]. These may be associated with jets, meanders, and eddies, seen to extend 100–400 km offshore in sea surface temperature images (from advanced very high resolution radiometer, or AVHRR) during spring through fall [*Ikeda and Emery*, 1984; *Flament et al.*, 1985; *Kosro and Huyer*, 1986; *Moum et al.*, 1988].

Both local wind stress and remote forcing affect the variability of the California Current. Sources of remote forcing include the inflow from the west wind drift at the north [*Chelton and Davis*, 1982], onshore transport of central Pacific water from the west [*Simpson*, 1984], Kelvin and coastally trapped waves propagating into the region from the south [*Spillane et al.*, 1987; *Pares-Sierra and O'Brien*, 1989; *Davis and Bogden*, 1989], and the oceanic component of the El Niño, also entering from the south [*Enfield and Allen*, 1980; *Chelton and Davis*, 1982]. Local winds over the California Current in the north (48°N) are primarily northward and are maximum in winter; in the south (25°–35°N) they are southward, on average, and maximum in late spring [*Nelson*, 1977; *Strub et al.*, 1987*a*]. At mid-latitudes (40°N), however, winds have a strong seasonal cycle consisting of relatively persistent southward winds in summer (with periods of relaxation) and intermittent northward (storm) winds in winter. *Strub et al.* [1987*b*] show the large spatial scale and short time scale of the spring transition in wind, sea level, water temperature and currents which separates the winter and summer regimes of the CCS. The spring transition was previously documented for the Oregon coast by *Huyer et al.* [1979]. This seasonality decreases at lower latitudes such that south of ≈ 34°N, winds are southward in both winter and summer. The average curl of the wind stress is positive in a narrow (100–200 km) band next to the coast and negative farther offshore [*Nelson*, 1977; *Rienecker and Ehret*, 1988]. The sign of the curl is consistent (through Sverdrup dynamics) with the general southward flow of the current and with the poleward undercurrent found over the continental slope *Hickey*, 1979; *Chelton*, 1984; *Pares-Sierra and O'Brien*, 1989].

2.2. *Biological Overview*

Temporal and spatial characteristics of chlorophyll concentration over the full extent of the CCS have not been documented. Numerous authors, however, have treated specific regions and/or time periods which are briefly reviewed here.

North of 48°N, *Thomas and Emery* [1986] show a strong relationship between winter (November–December) surface chlorophyll concentrations and hydrographic variables. Concentrations along the middle and outer shelf, in the northward flowing Davidson Current water, were < 0.2 mg m^{-3}. In summer, concentrations were > 5.0 mg m^{-3} in colder shelf water and < 1.0 mg m^{-3} in warmer, more stratified water over the shelf break and offshore [*Mackas et al.*, 1980; *Thomas and Emery*, 1988]. *Pan et al.* [1988] use CZCS data from 1979 to show the onset of a spring bloom in April, with elevated concentrations (≈ 1.0 mg m^{-3}) extending 100–200 km offshore. These offshore concentrations decreased in May. Maximum concentrations over the shelf were noted in August. These authors show that average monthly concentrations in regions ≥ 350 km offshore remain between 0.2 and 0.3 mg m^{-3} over the period March to September.

Off Oregon and Washington, *Landry et al.* [1989] review seasonal variation in chlorophyll concentrations using spatial averages from historical in situ data. Winter (November–February) surface concentrations are ≈ 1.0 mg m^{-3} in a region extending 90 km offshore. They report a spring bloom in March–April off Washington, with concentrations reaching 3.0 mg m^{-3}. They had insufficient data to document a bloom off Oregon. They do, however, show winter surface nitrate concentrations of ≈ 5.0 μM off both Oregon and Washington, indicating that light is probably limiting phytoplankton growth before March. Surface chlorophyll concentrations in areas greater than ≈ 70 km offshore have a midsummer minimum of ≈ 0.3 mg m^{-3}. Inshore of ≈ 40 km, concentrations are maximum ($>$ 3.0 mg m^{-3} off Oregon and > 6.0 mg m^{-3} off Washington) in summer months (May, June, and July) because of wind-driven coastal upwelling.

Spring and summer patterns of pigment concentration off central–northern California (38°–40°N) are strongly influenced by wind forcing, coastal features such as capes and possibly bottom topography in a region extending several hundred kilometers offshore [*Abbott and Zion*, 1987]. These authors show that both concentrations and variance are lower offshore and that there is a zone 50–70 km wide nearshore with concentrations greater than 2.0 mg m^{-3}. A close association exists between satellite-measured pigment concentrations, satellite measured sea surface temperature, and surface nutrient distributions in this region of strong summer upwelling [*Traganza et al.*, 1983; *Abbott and Zion*, 1985]. The seaward edge of high pigment concentrations off central–northern California is highly scalloped in summer and numerous mesoscale features are visible in individual satellite images, suggesting a dynamic interaction between the recently upwelled water next to the coast, the southward jet of the CCS and more oligotrophic waters of the central Pacific [*Abbott and Zion*, 1985; *Peláez and McGowan*, 1986; *Haury et al.*, 1986; *Simpson et al.*, 1986].

Both spatial and temporal variability of pigment concentration off southern and central California have been studied using CZCS data by *Smith et al.* [1988], *Michaelsen et al.* [1988], and *Peláez and McGowan* [1986]. A gradient from high concentrations nearshore to low concentrations offshore persists throughout the year. These data are supported by zonal transects of in situ measured surface chlorophyll concentration reported by *Mullin* [1986] and *Haury et al.* [1986]. In general, concentrations are greater than 2.0 mg m^{-3} within 25 to 50 km of the coast and decrease to < 0.5 mg m^{-3} at distances greater than 200 km. A distinct latitudinal difference in nearshore pigment concentrations off southern California is noted by *Smith et al.* [1988]. Concentrations north of Point Conception have a higher mean and lower temporal variance than concentrations in the Southern California Bight. The eastward intrusion of water into the bight described in section 2.1 is very low in nutrients and chlorophyll, as was documented by *Peláez and McGowan* [1986]. These authors also show a seasonally varying tongue of high pigment concentration which extends south of Point Conception offshore of the bight. From individual CZCS images in 1981 and 1982 they show that this tongue extends farthest south in August or September and is less well defined and farther north in fall and winter. Data from *Haury et al.* [1986] suggest that offshore regions of higher biomass southwest of Point Conception might be the result of advection from coastal areas of high productivity. An alternate explanation for the position of this tongue is given by *Chelton et al.* [1982], who show this region to be coincident with an offshore maximum in zooplankton biomass where upwelling by Ekman pumping is suggested by positive wind stress curl.

Eppley et al. [1985] use in situ measurements to show that the annual cycle in total water column primary production is weak in the Southern California Bight but that chlorophyll concentrations in the upper attenuation depth are maximum in winter. In winter, phytoplankton are evenly distributed within the mixed layer, but during spring and summer a subsurface maximum develops [*Cullen and Eppley*, 1981] below the depth where the satellite can measure. While chlorophyll integrated over the euphotic zone has a maximum in spring and is higher in summer than winter, chlorophyll concentrations in the upper attenuation depth (that measured by the CZCS) have a winter maximum and a summer minimum [*Michaelsen et al.*, 1988]. Winter maxima in satellite color data will be due to this artifact of the depth of sampling [*Campbell and O'Reilly*, 1988] as well as to an error in the atmospheric correction algorithm at large solar zenith angles. This error is discussed in detail in the next section and in Appendix A.

3. Data and Methods

3.1. *Satellite-Derived Chlorophyll*

Coastal zone color scanner data of the region 20°–55°N, 105°–140°W were recorded at the Scripps Satellite Oceanography Facility (SSOF) for the period July 1979 to June 1986 and processed at the Jet Propulsion Laboratory (JPL) to form the west coast time series [*Abbott and Zion*, 1985]. Details of the processing can be found in Appendix A, along with a discussion of the sources of error. In the present analyses, the mosaic fields (7-km resolution) were used to form monthly means of surface pigment concentration in 1° blocks (Figure 1). Higher cross-shelf resolution was obtained in the 100-km region next to the coast, where monthly means were also formed for blocks 1° in latitude and 25 km wide in the east-west direction.

The approach taken here is to assume that the data set contains the signals of interest along with both systematic and random errors. After screening the images visually for obvious errors, we first identify a systematic bias in the data, which we believe is due to an incomplete removal of atmospheric scattering effects (see below and Appendix A). After removing this bias, random and undetected systematic errors remain in the data. The effects of random errors are reduced by the temporal and spatial averaging. The methods of empirical orthogonal function (EOF) analysis and principal estimator pattern (PEP) analysis are used to extract the biological signal from the noise and to relate the anomalous pigment concentrations to surface wind forcing (Appendix B).

3.1.1. *Effects of errors in the data.* Although the statistical methods used should separate the large-scale signal from the random noise, they may not remove the effects of undetected systematic errors. Thus before proceeding, we discuss ways in which the sources of error (described in Appendix A) might appear in the results.

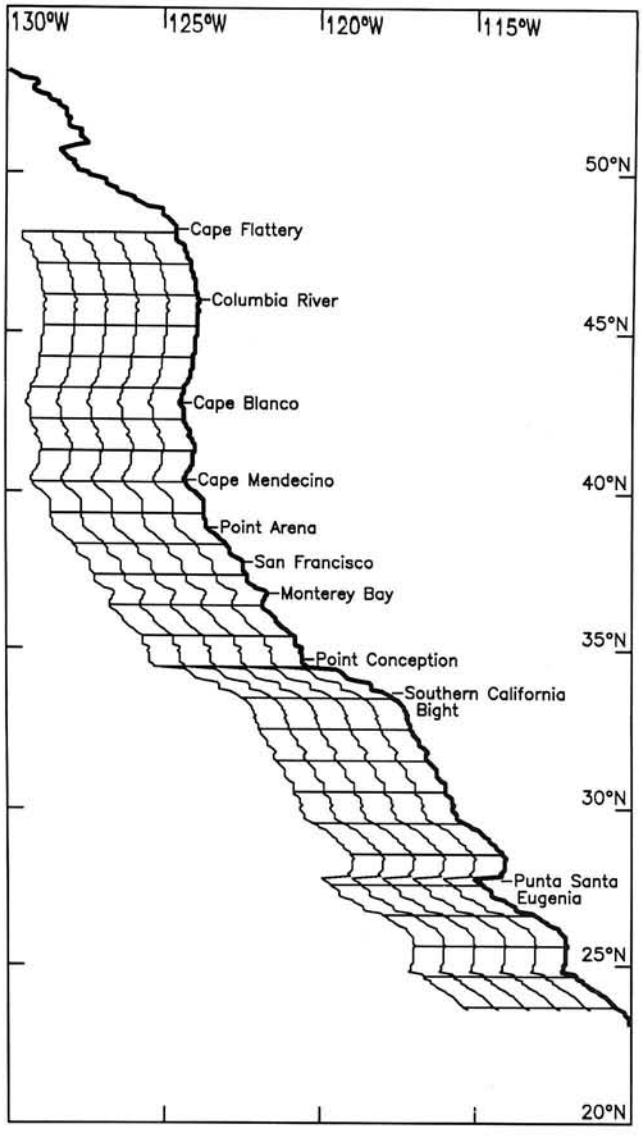

Fig. 1. Coastal outline, derived from the satellite imagery, showing the geographic points referenced in the text. Also shown are the 1° × 1° bins used to average pigment data over the large-scale CCS. Using Point Conception as the starting point, the coast was divided into 1° latitude sections. The offshore boundaries of the bins are multiples of 1° in longitude from the coast in the E–W direction.

Sensor degradation: An overall decrease in the sensitivity of the sensor occurred over the course of the mission, and a correction function is included in the Miami processing software to account for this. This change in sensor sensitivity happened at specific times, rather than gradually. Thus although the correction for the long-term trend in sensor degradation is believed to be good, short-term changes may not be well accounted for. If an incorrect long-term correction remains in the data, we expect to see a trend over the whole data set that would be evident, for instance, in the time series of the EOFs. Short-term shifts in the sensitivity would not be obvious and the suggestion has been made that absolute pigment concentrations in individual images should be considered good to a factor of 2 [*R. Evans*, personal communication, 1989]. Temporal averaging may help reduce the size of abrupt changes and also reduce any effect of alternating bias in the sensor. The change in sensitivity would affect whole images and would not change spatial relationships within the image. It would also not be correlated with other physical variables, such as wind, and would thus tend to be eliminated by the PEP analysis, which brings out the spatial patterns of pigment concentration that vary in concert with spatial patterns of the wind variables.

Cloud screening: As is described in Appendix A, clouds may not have been correctly identified in some cases. Temporal averaging will reduce this effect for cirrus and cumulus, which have an approximately random distribution along the west coast. In summer, however, a bank of stratus clouds often lies offshore, with a band of clear water next to the coast. Undetected subpixel-sized clouds next to this stratus bank would systematically affect a north-south strip some distance offshore. Since the position of the cloud bank changes in time, temporal averaging will both reduce this effect and smear it over a wider region. The orientation of this error, however, should still be in a north-south band.

Cloud ringing: The failure of the sensor to recover immediately from saturation after viewing bright clouds causes incorrect chlorophyll values to the east of clouds for distances of up to 70 km [*Mueller*, 1988]. *Eckstein and Simpson* [1990] estimate errors of $\geq$40% from this source. The algorithm of Mueller was used in the WCTS processing to produce a cloud mask to indicate where data might be affected. In the present study this mask was examined for a number of images but was not used in the final analysis, since it was found to eliminate more data than was necessary. Thus effects of cloud ringing remain in the data. Temporal averaging will reduce the effects of random clouds (cirrus and cumulus), but the presence of the stratus bank offshore in summer will again provide a source of systematic error which should have a north-south banded nature. Regions to the east of islands may also be affected, although no emphasis is placed on the few such regions in our area.

Atmospheric scattering: Both Rayleigh and aerosol (Mie) scattering increase the radiances seen by the satellite. The problem is most severe when the angle formed by the satellite, the sun, and the viewing point beneath the satellite is large (a value of 50° is often used as a rough limit). This occurs in winter at high latitudes. The single-scattering Rayleigh algorithm used in the WCTS processing produces winter values of chlorophyll known to be too high. The multiple-scattering Rayleigh algorithm used in processing the global CZCS data is better [*Gordon et al.*, 1988*a*], but may still create systematic biases in winter at high latitudes (see below). If only Rayleigh (molecular) scattering were involved, the symptoms of this error would be fairly simple, i.e., uniformly increasing chlorophyll with latitude and with a seasonal maximum in winter. These properties are used to form a crude empirical correction function for the scattering errors below. Errors in the aerosol scattering are not as easily accounted for.

Uniform aerosols: The WCTS was processed using the clear water procedure with uniform values of $\epsilon = 1$, on the assumption that all aerosols are identical marine aerosols (Appendix A). Errors occur where winds blow continental type aerosols over the ocean. If these winds have synoptic (3–5 days) time scales, monthly averaging will reduce these errors. North of 35°N, winds are usually from

the southwest or the northwest during the passage of synoptic weather systems from fall through spring. During clear periods in spring through fall, a diurnal sea breeze develops which includes onshore winds at midday and in the afternoon [*Beardsley et al.*, 1987] at the time of the CZCS image. Thus, during much of the year, the wind flow off the west coast is onshore and the assumption of uniform marine aerosols is reasonably valid. Regions where this may not be true include the Southern California Bight during extended periods of Santa Ana (offshore) winds. At present, there is no consistent solution to this problem using the WCTS. Individual investigators interested in specific regions may be able to tune the values of ϵ used to process raw images for specific regions and times. Use of this approach in the WCTS processing, however, would have introduced an unacceptable level of subjectivity into the final product. Consistency of processing was one of the goals of the processing. Attempts to adjust the values of ϵ on a scene-by-scene basis during tests of the global CZCS processing resulted in greater errors than assuming uniform marine aerosols, which was the final procedure adopted in that processing as well [*G. Feldman*, personal communication, 1989].

An estimate of the cumulative effect of these errors in our region comes from *Abbott and Zion* [1985], who find that WCTS estimates of surface pigment concentration from individual images off northern California are roughly within a factor of 2 of in situ values. This is the same level of error found in other regions [*Gordon et al.*, 1983*a*, 1988*b*; *Denman and Abbott*, 1988; *Balch et al.*, 1989*b*] and suggested for the global CZCS data set [*R. Evans*, personal communication, 1989]. The temporal and spatial averaging used in the present study should reduce some (not all) of the effects of errors described above.

3.1.2. *An empirical correction function.* The most serious systematically identifiable problem in the WCTS comes from the single-scattering Rayleigh algorithm. We have attempted to reduce this error by forming a correction function based on the assumption that true chlorophyll levels are low some distance from the coast for most of the year [*Thomas and Emery*, 1986; *Landry et al.*, 1989; *Haury et al.*, 1986]. A 2.5° wide band of the CZCS data separated from the coast by 2.5° longitude and extending from 25°N to 50°N is used to define a region where we expect the true annual cycle of surface pigment concentration to be low and the apparent annual cycle in the WCTS to be dominated by the Rayleigh scattering error. This region consists of the western half of the domain shown in Figure 1. We expect the error to increase to the north and to be maximum in December. The first EOF of the data in this band accounts for 70% of the variance and has the temporal and spatial characteristics expected of the Rayleigh scattering error (Figure 2*a*). The product of the temporal and spatial functions is used as a first-order correction function (dependent on month and latitude). In the analyses presented below, we will always note when this empirical correction function has been used.

The general effect of subtracting this correction function from the monthly CZCS data is shown by performing an EOF analysis on the raw, monthly 1° mean WCTS pigment data (no empirical correction or seasonal cycle removed). Figure 2*b* shows the spatial pattern and mean monthly time series of the first EOF of the uncorrected data. It is dominated by the north-south gradient seen most clearly at the offshore edge and by a cross-shelf gradient, with higher values offshore. The time series peaks in December–January. Figure 2*c* shows the first EOF calculated from the same data after removing the latitude and time dependent function shown in Figure 2*a*. What appears now is the development of the band of high pigment near the coast in summer. This is one view of the annual cycle in surface pigment. It represents that part of the seasonal cycle that can be represented by one spatial pattern and accounts for 36% of the variance in the monthly, corrected, 1° averaged WCTS data.

The WCTS will eventually be reprocessed with the multiple-scattering Rayleigh model, which has been used in the global CZCS processing. To determine whether this new version of the WCTS will produce results different from those derived below for the empirically corrected WCTS data used here, we obtained the monthly composites of the global data set (processed with the multiple-scattering algorithm) for the period November 1978 to June 1981. This is the period for which the sensor was most stable [*R. Evans*, personal communication, 1989]. Thus we have WCTS and global data for a common period of 2 years, July 1979 to June 1981. Comparisons of the annual cycles derived from these 2 years from the corrected WCTS and the global CZCS data are presented in section 4.1 in support of the argument that the major conclusions about the seasonal development for the March–October period based on the corrected WCTS will not be changed when the

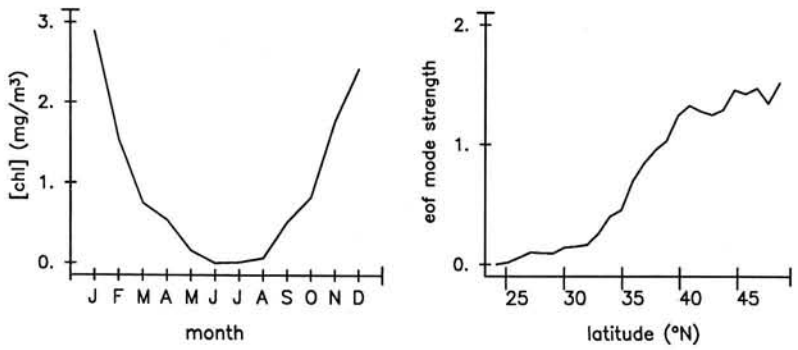

Fig. 2*a*. The first EOF of an offshore band of pigment concentration, accounting for 70.6% of the variance. The time series has been averaged by calendar month. This EOF is used as the correction function to reduce effects of errors in the scattering algorithm.

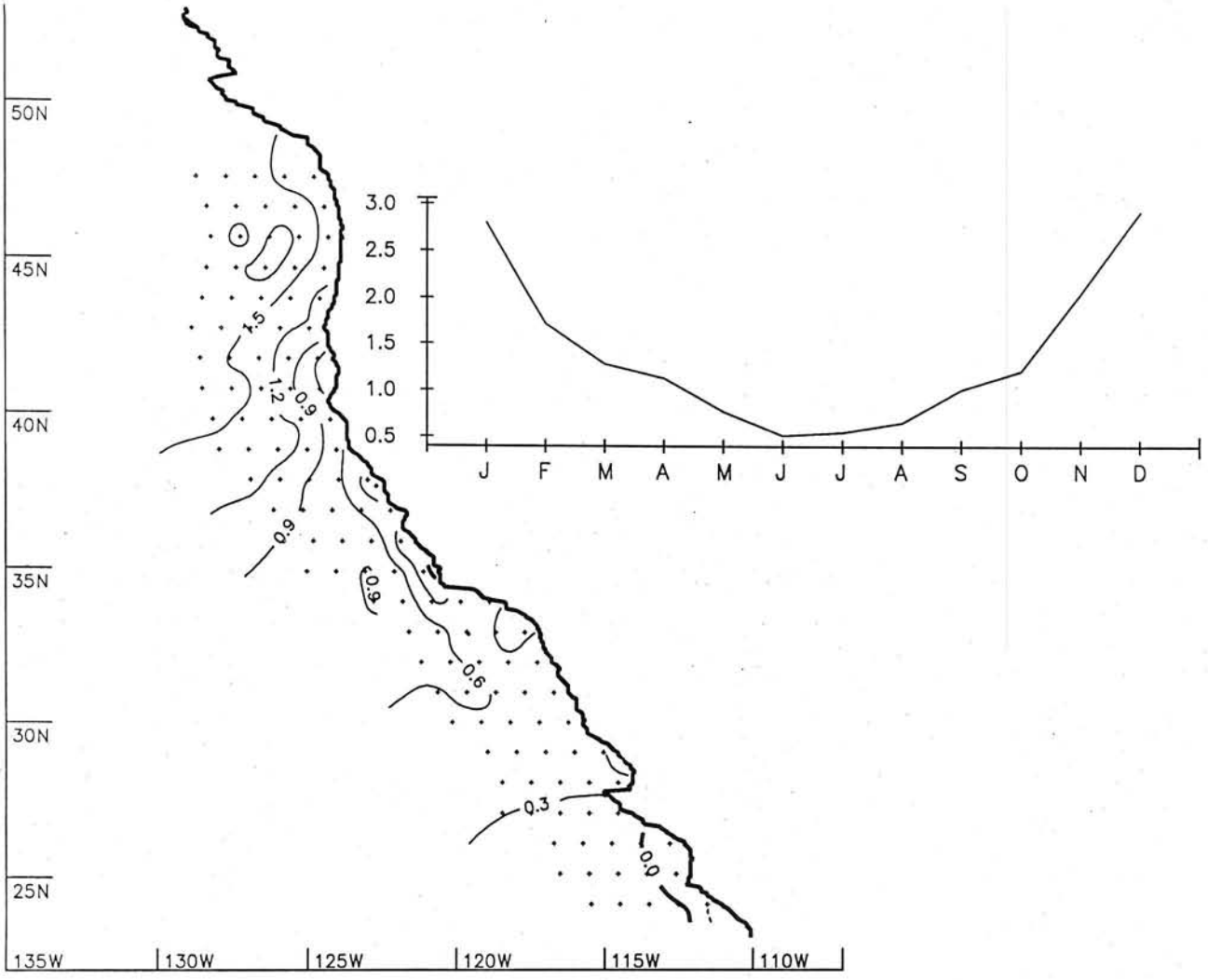

Fig. 2*b*. The first EOF of the monthly pigment data, with no correction applied and no seasonal cycle removed, accounting for 85.4% of the variance. The time series has been averaged by calendar month.

data are eventually reprocessed with the multiple-scattering algorithm.

If the error in the scattering algorithm were only a function of latitude and season, it would be part of the monthly seasonal cycle at each location and would not affect the monthly anomalies, which are formed by removing the seasonal cycle at each location. The initial EOF analysis of the CZCS anomalies, however, was dominated by spatial modes concentrated in the north, with temporal peaks in one or two winters. We cannot determine whether this is caused by actual winter phytoplankton dynamics or interannual differences in atmospheric properties. For this reason we exclude the 4-month winter period November–February in each year from the final data set used in the statistical analyses of anomalous CZCS. With the additional exclusion of 1984 due to lack of data (see below), the monthly pigment time series consists of a total of 48 time points from July 1979 through June 1986.

3.2. *Wind Data*

The surface wind data come from National Meteorological Center's Limited-Area Fine Mesh (LFM) 6-hour forecasts, archived at the National Center for Atmospheric Research. These fields are formed at 12 hour intervals on a polar stereographic grid with 190-km spacing at 60°N. Since sampling by merchant ships is insufficient to calculate reliable curl fields and buoy coverage is neither continuous nor spatially suited to curl calculation, products such as the LFM fields must be relied on, with attention to the degree to which they represent the true variability in the wind.

We consider three wind variables: wind stress ($\vec{\tau}$), curl of the wind stress, and u_*^3, where $u_*^2 = |\vec{\tau}| / \rho_a$. The alongshore wind stress (τ_a) at the coast represents an index of coastal upwelling [*Bakun*, 1973]. The curl of the wind stress represents an index of offshore upwelling due to Ekman pumping. The variable u_*^3 represents the wind energy available for vertical mixing. Windstress is formed from winds using a standard bulk formula, with a constant drag coefficient of $c_D = 1.3 \times 10^{-3}$ and a constant air density of $\rho_a = 1.3$ kg m^{-3}. The analyses consider two-dimensional fields of the wind variables and a one-dimensional coastal strip of wind variables, interpolated to points 0.5° from the coast and separated by 1° in the alongshore direction (the centers of the 1° × 1° CZCS blocks next to the coast in Figure 1). In the coastal strip, the alongshore component of the wind stress (defined

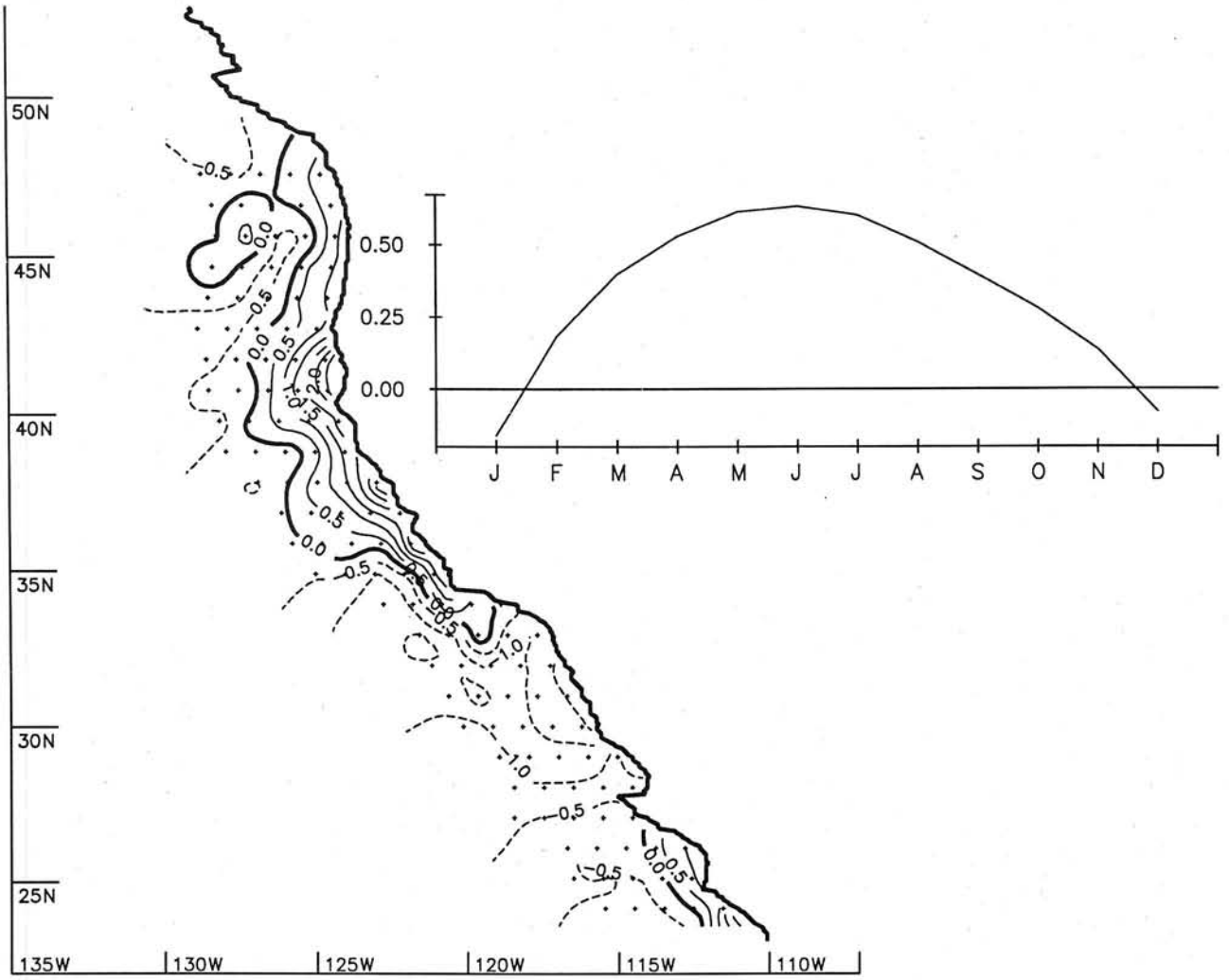

Fig. 2c. As in Figure 2b for the same data corrected by subtracting the function shown in Figure 2a. This EOF accounts for 36.2% of the corrected monthly variance and describes the mean seasonal cycle.

by the coastal orientation) is used as the indicator of upwelling.

An evaluation of the 12-hour LFM winds was made by correlating them with winds observed at eight National Data Buoy Center (NDBC) buoys in 1981–1983. The average correlation coefficients for (u, v) components were (0.60, 0.80) in spring, (0.55, 0.73) in summer, (0.70, 0.87) in fall, and (0.70, 0.83) in winter. These winds thus explain 50%–70% of the variance in twice-daily winds in the N–S direction and 30%–50% of the variance in the E–W direction. The variability of the monthly average fields is much less, increasing the correlations.

Fields of wind stress curl calculated from the LFM data were evaluated by comparing them to similar fields calculated from ship winds by *Nelson* [1977] and *Rienecker and Ehret* [1988]. These were qualitatively similar, except for the absence (in the LFM fields) of a band of positive curl off Oregon and Washington in summer. This is thought to be a failure in the LFM winds and the same failure is found in the Navy's Fleet Numerical Oceanographic Center (FNOC) wind fields. Values of the wind stress curl are also lower (by roughly a factor of 5–10) than those calculated from ship and buoy winds separated by 25–150 km, reflecting the relative smoothness of the LFM winds on scales of 100–200 km.

There may also be a displacement of the large-scale features in the LFM wind fields. This was noted in considering the winds calculated from FNOC operational surface pressure fields by *Bakun* [1973]. The summer maximum in southward winds was found to occur too far to the south in the operational FNOC wind product because of an overestimate of the effect of the thermal low over southern California and Mexico, producing the correct temporal development but an error in the spatial placement of the maximum. In comparing wind variables to satellite pigment concentrations using either point correlations or the PEP patterns, we must keep in mind the possible displacement or distortion of the spatial features of the wind fields. This could cause an apparent correlation of the LFM winds in one region with the pigment response in a separate region, whereas the real winds and pigment response may have been coincident in space.

3.3. *Statistical Methods*

Time series of CZCS and wind data cover the period July 1979 to June 1986. Monthly means of CZCS pigment were formed on the original mosaic grid ($0.07^\circ \times 0.07^\circ$). These were then averaged over the $1^\circ \times 1^\circ$ blocks shown in Figure 1 extending 5° offshore; data in the region

next to the coast were also averaged into four 1° latitude by 0.28° (25 km) longitude blocks. Even with this spatial and temporal averaging, gaps comprising 10% of the total data occur in the CZCS time series, usually covering only 1–2 months at a time. For each location, gaps were filled by optimal interpolation in time, using an exponentially damped cosine fit to the autocovariance function determined from the data at that location. Very few images were recorded during 1984 and we exclude this year from the time series analyses. Excluding 1984, only 7% of the data set was filled by interpolation. A monthly seasonal cycle was formed from 6-year means of the calendar months at each location and subtracted from the monthly means to form monthly anomalies.

Wind variables were calculated for each 12-hour period on the original LFM grid and averaged into monthly means. The wind variables for each 12-hour period were also interpolated to the centers of the CZCS 1° × 1° blocks closest to the coast and averaged into monthly means. The seasonal cycles and monthly anomalies of the wind variables were formed in the same manner as for pigment concentrations.

Empirical orthogonal functions (EOFs) were formed for all variables, using the covariance matrices of the monthly anomalies [*Richman*, 1986]. The method of principal estimator patterns (PEPs), also known as canonical correlation analysis, was used to test the statistical connection between each wind variable and the CZCS pigment field [*Hotelling*, 1936; *Davis*, 1977, 1978], using lags of 0 and 1 month between wind variables and pigment concentration. This method calculates the skill of the wind variables in predicting the pigment concentration, as the percent of variance explained. Use of the 1-month lag between wind and pigment did not improve the statistics and is not discussed further. To assess whether this skill was greater than that expected for random variables, the calculation was repeated for lags greater than 6 months, for which any statistical relation between monthly anomalies is assumed random. The average percent of variance explained for these long lags is referred to as the artificial skill. Further details of the PEP method are described in Appendix B.

4. Results

4.1. *Seasonal Cycle*

The 6-year means of pigment concentration for the calendar months March–October on the mosaic grid are shown in Plate 1. The time and latitude dependent correction function (Figure 2*a*) has been subtracted from these data. Locations where the correction produces pigment concentrations less than or equal to 0 are shown in white. Figure 3 shows the number of years of data used to form the mean at each grid point for each calendar month. Data availability is generally good (4–6 realizations) near the coast for March through May and August through November. Winter is poorly represented in the north due to cloud cover; relatively poor sampling in June and July is due to a midsummer annual minimum in power supply aboard the satellite.

The seasonal progression in Plate 1 shows that in March a diffuse region of higher pigment concentration (1–2 $mg\,m^{-3}$) extends several hundred kilometers offshore from southern Oregon to Point Conception. The width of this region is reduced between May and June. In June the narrow pigment maximum develops a strongly meandering offshore edge which continues into July. The nature of the June and July means may reflect the fact that most of the data available in these month came from just 2 years, 1980 and 1981. The width of the high pigment concentration region expands in August and September as the very high nearshore values decrease. Smaller-scale features are also evident in Plate 1. A narrow band of high pigment concentration is present north of the Columbia River (46°N) in April–May, decreasing in June and reappearing in July–October. A region of apparently high pigment is present in all months around the San Francisco Bay (37.5°N). A band of high pigment concentration extends southeast of Point Conception. Low pigment concentrations are seen within the Southern California Bight during most months. Note the general similarity between the spatial structure of the first EOF of corrected WCTS data in Figure 2*c* and the summer pattern in Plate 1.

Figure 4*a* presents the mean annual evolution of the latitudinal structure of pigments in alongshore bands of 25 km and 100 km width next to the coast and 50 km and 200 km width farther offshore. (Note that for this discussion, distance "offshore" is defined as distance in an east-west direction. This definition may be misleading in the Southern California Bight, where points identified as 100–300 km offshore are closer than that to the shore in a northward direction.) The correction function (Figure 2*a*) has been subtracted from the data (reducing winter values in the north), and the full WCTS period (excluding 1984) has been used to form the mean calendar months at each location. Because of errors in the atmospheric correction, data from November to February should be disregarded in favor of the center portion of each year between the vertical lines.

The 25 km closest to the coast (Figure 4*a*, bottom right) is the region most influenced by coastal upwelling, mixing associated with bottom topography and river input, which may create case II water conditions (see Appendix A). In this region there is an increase in pigment concentration north of approximately (46°N) in April–May, a decrease in June and another increase in July (also apparent in Plate 1). The early increase is delayed and lower off Oregon (42°–46°N). Off northern California, pigment concentrations increase first off San Francisco (37°–38°N) in March, then everywhere from Point Conception to Cape Mendocino (35°–42°N) in April–May. The increased pigment values move north and appear off Oregon in June–August. Lower pigment values are found in the Southern California Bight (32°–34°N) with a relative maximum in March–April and a minimum in late summer and fall. Off Baja California, there is a region of higher pigment concentration south of 32°N with peaks around the two major capes (25°N and 28°N) in late spring and early summer, followed by a minimum in late summer and fall, similar to that in the bight to the north.

Most of the above features are found in the 25 to 75-km band (Figure 4*a*, bottom left) with lower concentrations in this area farther from the coast. This band is mostly offshore of the continental shelf, in deep water. This region clearly shows the low values found most of the year off southern California and northern Baja (30°N to 33°N), with a relative minimum in August. A late

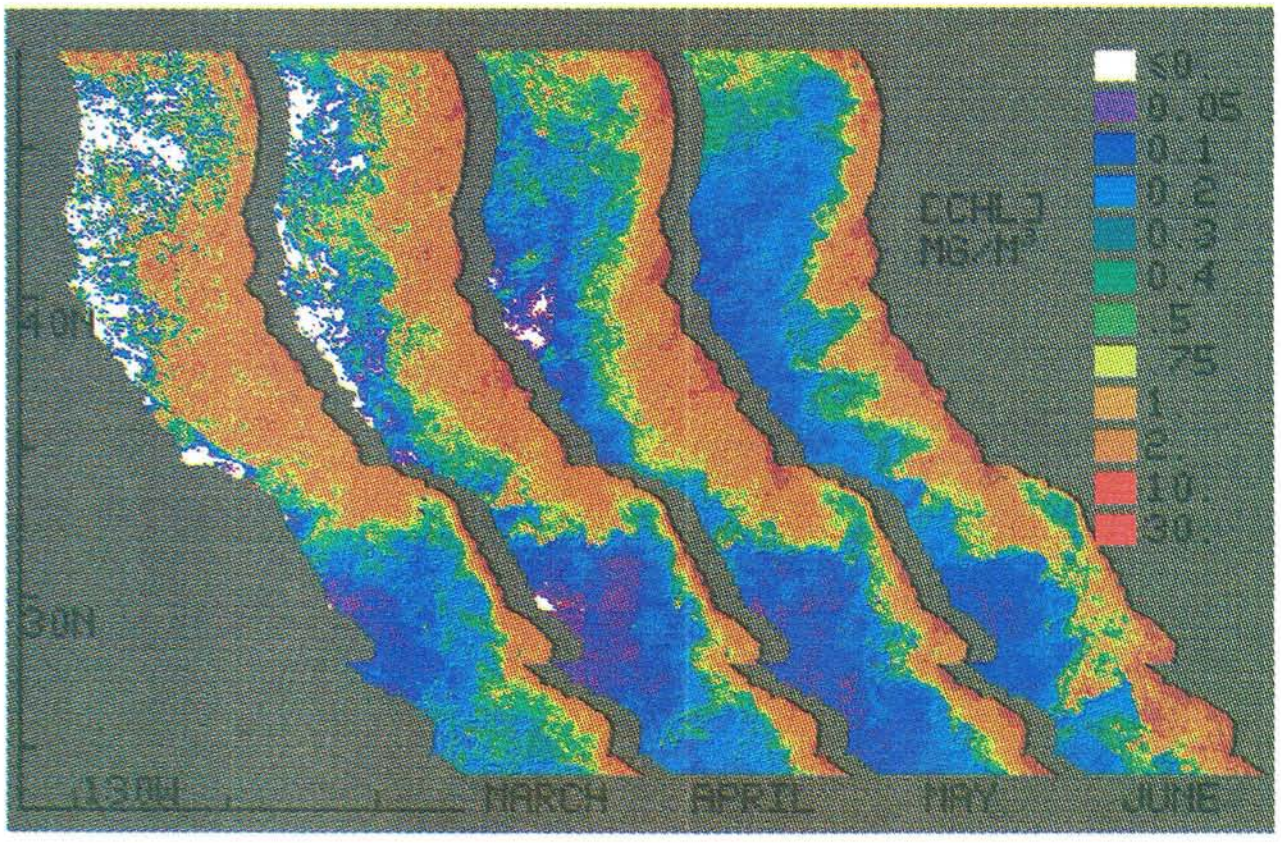

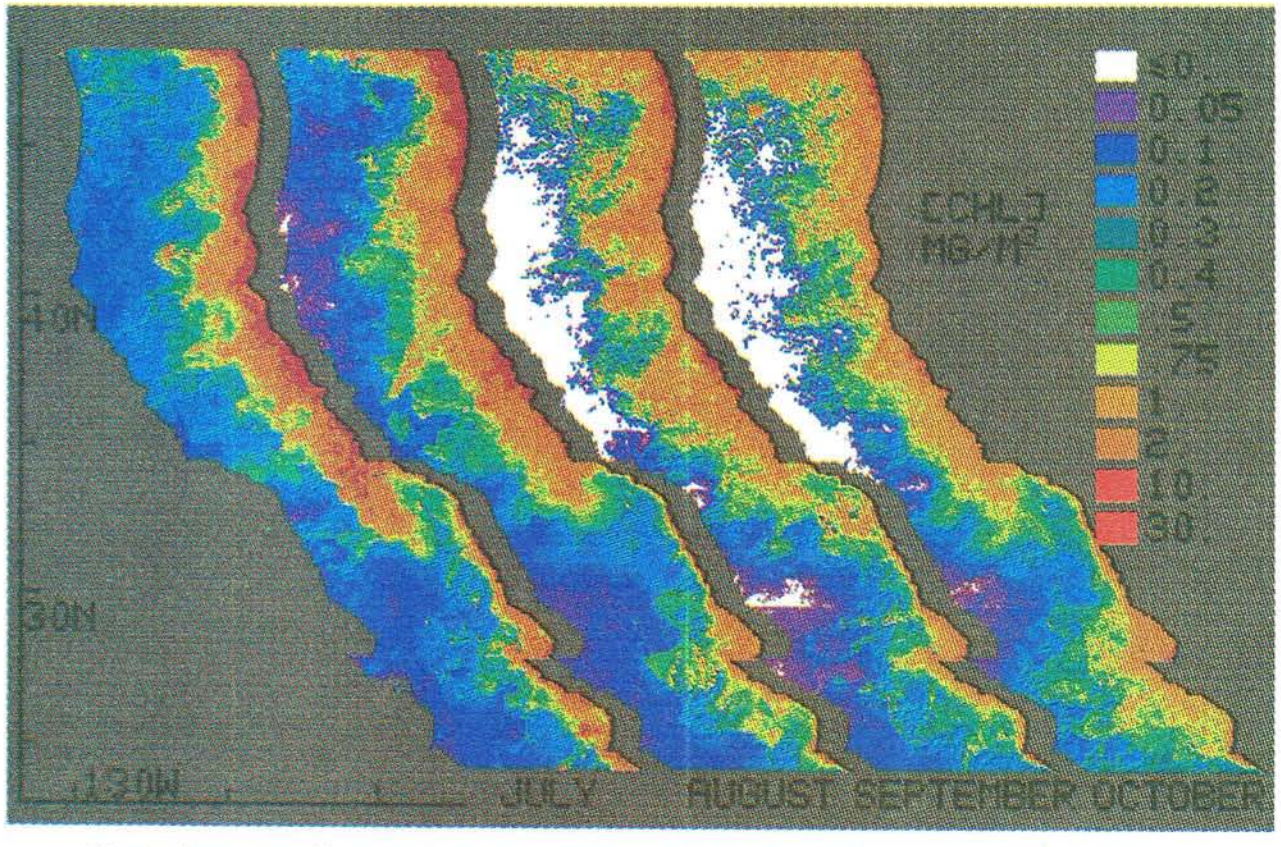

Plate 1. Six-year monthly mean pigment concentrations for March–October (July 1979 to June 1986, excluding 1984). Resolution is 0.07° × 0.07° (WCTS mosaic grid). The correction function (Figure 2a) has been used, reducing values in the north in winter. Values reduced to less than 0 are colored white (values in the color bar are in milligrams per cubic meter).

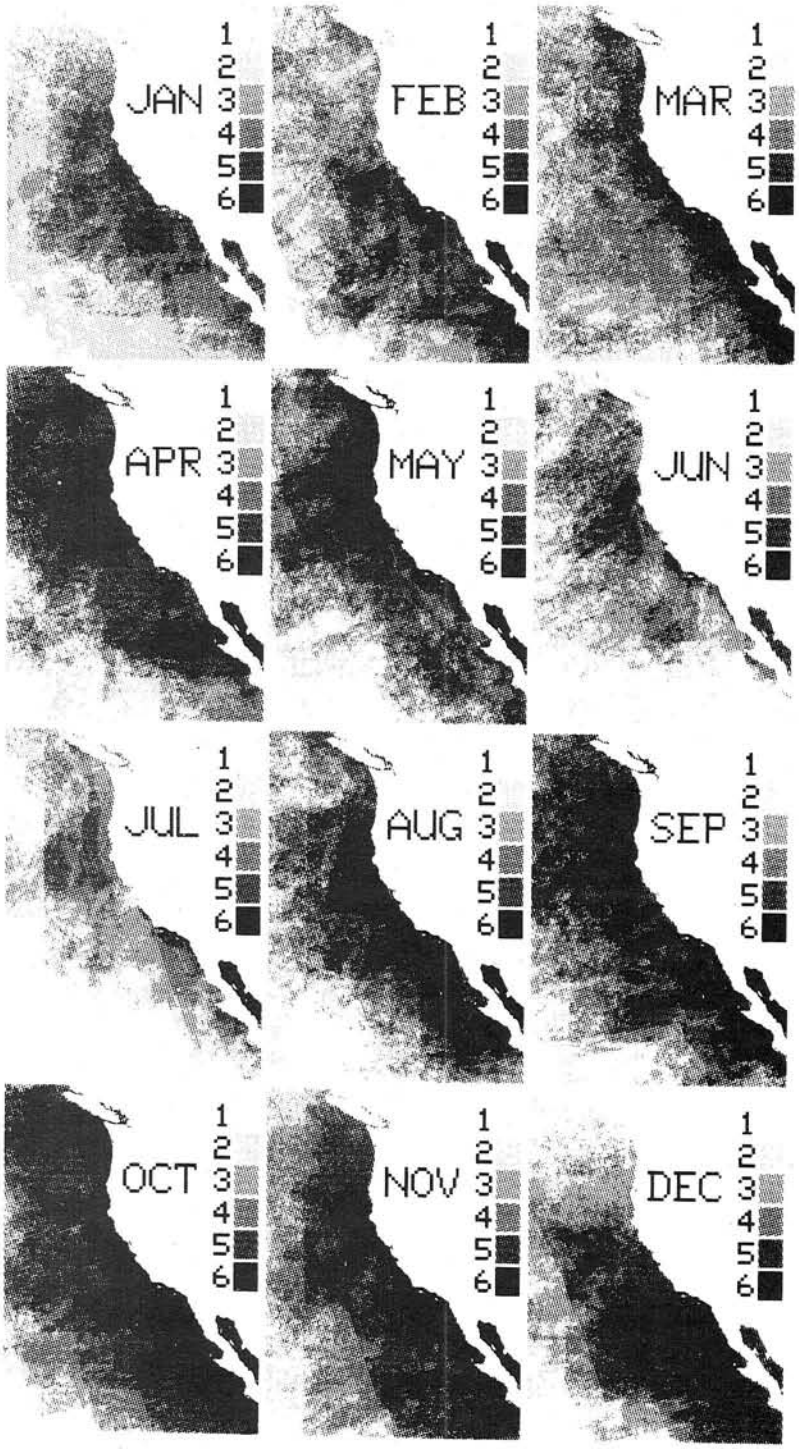

Fig. 3. Number of months of data used to form the monthly means in Plate 1.

summer maximum appears off Washington in August. The wider coastal band from 0–100 km offshore (top right) provides a smoother picture of seasonally varying pigment concentration in the large-scale coastal ocean next to North America. Farther from the coast, in the band between 100–300 km offshore (top left), there is a small increase in pigment everywhere north of 33°N in early spring, maximum and longest lasting at 34°N and 37°N–38°N. Between 300–500 km offshore (not shown) the only feature is a brief and weak (<0.5 $mg\,m^{-3}$) spring bloom off California, lasting longest between 32°N and 35°N where advection from north of the Southern California Bight brings coastal water into this band.

To assess whether use of the multiple-scattering Rayleigh correction would change the picture derived from the corrected WCTS data, similar annual cycles are formed from the available global CZCS data for the period July 1979 through June 1981 and presented in Figure 4*b*;

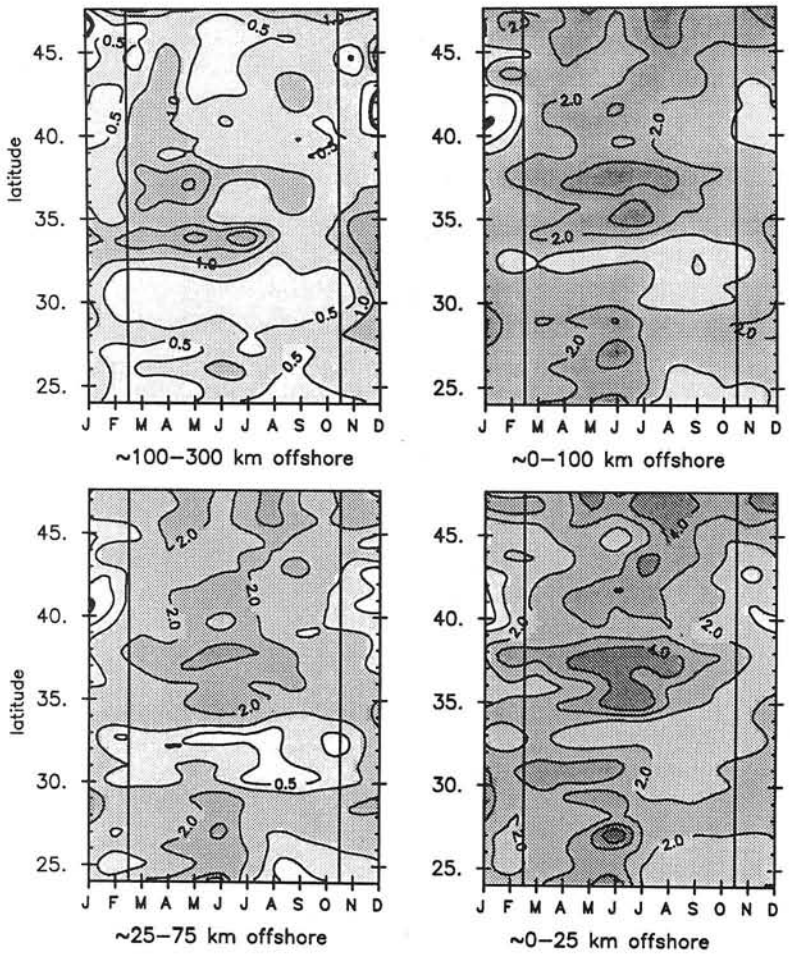

Fig. 4*a*. Seasonal cycles of surface pigment concentration (mg m^{-3}) in different offshore bands, contoured as a function of latitude and month. The band from ≈ 0–100 km offshore (top right) is the 1° band closest to the coast in Figure 1; the band from ≈ 0–25 km offshore is a similar coastal band 0.28°wide, etc. These seasonal cycles are formed from the full WCTS data set (excluding 1984). The empirical correction function (Figure 2*a*) has been subtracted from this data.

these can be compared in general with Figure 4*a*. To provide a direct comparison, the corrected WCTS data from the same 2-year period used in Figure 4*b* are shown in Figure 4*c*. When comparing Figure 4*a* with either 4*b* or 4*c*, it should be kept in mind that the complete time period used in Figure 4*a* includes a major El Niño, during which pigment values were lower than usual, especially south of the Columbia River. The years 1980 and 1981 also had stronger spring transitions than the other years, with high pigment concentrations far offshore [*Thomas and Strub*, 1989].

Many of the prominent features in Figure 4*a* are found in Figures 4*b* and 4*c*, with a few exceptions. In the 0- to 25-km and 0- to 100-km bands (bottom and top right), the early spring bloom and subsequent decrease in pigment concentration is seen off Washington and northern Oregon, but the second summer increase off Washington is weaker in the global data than in the corrected WCTS. Details of the summer maxima also differ between Figures 4*b* and 4*c*, but both show the progression of increased pigment concentration from northern California to Oregon in the 100 km next to the coast in the second half of summer. Data from the global data set show maxima more localized in Figure 4*b* than the corrected WCTS in Figure 4*c*, which seems to miss the maximum between Capes Mendocino and Blanco (41°N) in spring of these 2 years, especially over the shelf (bottom right). These differences may reflect the fact that the WCTS and the global data sets were constructed from different sets of images, in addition to the use of the multiple-scattering algorithm and a more detailed sensor degradation correction function. Data from this 2 year period between 0–25 and 25–75 km offshore show the maximum off Oregon in late summer to be more localized around Cape Blanco (most clearly seen in Figure 4*b*). Pigment concentrations are lower south of 33° in the global data set than in the WCTS, reflecting the apparent failure of the empirical correction function in the south. The global data in Figure 4*b* are more like the corrected WCTS from the full period in Figure 4*a* and clearly show the low seasonality and low concentrations in the Southern California Bight. In the global data within 100 km of the coast, the minimum in late summer appears more as a spring increase south of 32°N and north of 33°N, followed by a decrease in late summer between 28°and 33°N. The late summer minimum is not as evident in the corrected WCTS from this 2-year period, indicating that this feature of the 6-year mean (Figure 4*a*) comes mostly from the 1981–1983 and 1985 period. It is of interest

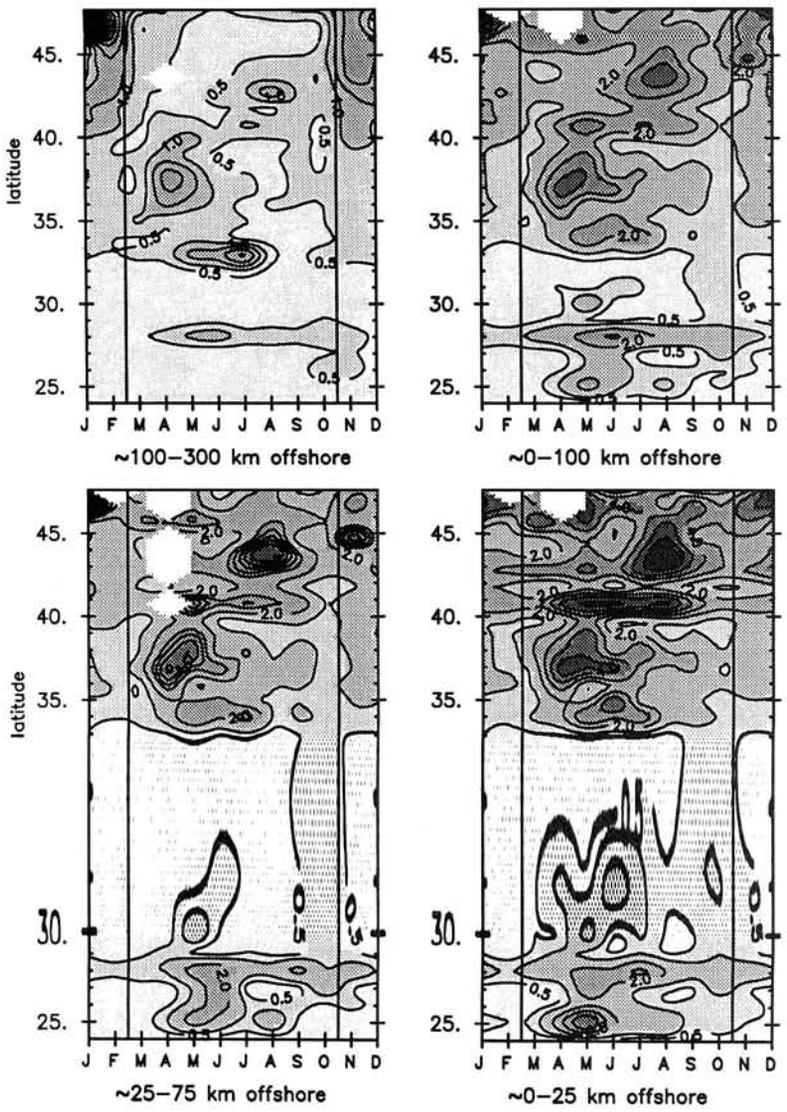

Fig. 4*b*. Seasonal cycles, as in Figure 4*a*, except formed from monthly composites from the global CZCS data set for the two-year period July 1979 through June 1981. No correction function has been applied.

that the global data show a systematic increase in pigment concentration in November through February in the region from 100 to 300 km offshore (Figure 4*b*, top left) and increasing north of approximately 33°N, suggesting that the improved scattering algorithm has not solved all of the problems with winter data at high latitudes.

An alternate method of looking at annual cycles is to fit annual and semiannual harmonics to the time series at each point [*Chelton*, 1984; *Strub et al.*, 1987*a*]. The disadvantage of this method is its inability to represent abrupt seasonal changes. The advantage, however, is that it allows one to calculate the significance of the seasonal cycle using bootstrap statistics, i.e., the probability that a random data set would fit the harmonics as well [*Strub et al.*, 1987*a*; *Michaelsen et al.*, 1988]. We have fit annual and semiannual harmonics to the corrected WCTS data used to form Figure 4*a* and reconstructed plots of the annual cycles similar to those presented in Figure 4*a*. In general, the annual cycles look very much like Figure 4*a*, except for the lack of short or closely spaced features, such as the double maximum off Washington in summer. In Figure 4*d* we present the latitudinal distribution of the coefficient of determination (fraction of variance explained) for the multiple regression of annual and semiannual harmonics in the four bands shown in Figure 4*a*. Also presented are the bootstrap estimates of the 95% significance level, averaging around 0.1. For the regions within 100 km of the coast, the results show the fits to be significant for latitudes south of 28°N and between 34° and 43°N, where the fits account for 30–50% of the monthly variability. The failure of the fits north of 43° may reflect shorter period fluctuations such as the double summer maxima there. The failure of the fits in the region between 28° and 33°N reflects the very low degree of seasonality in the Southern California Bight and off Baja California north of Punta Eugenia.

4.2. *Nonseasonal Variability*

4.2.1. *Point correlations.* The simplest test of the relation between anomalies of monthly wind variables and pigment concentrations consists of point correlations of the time series. The general result of these tests is that monthly anomalies of pigment concentration are very marginally correlated with local alongshore wind stress in a few nearshore locations and are significantly correlated with local u_*^3 in some offshore regions and wind stress curl in some nearshore regions. Only 16–24% of the variance in these limited regions is accounted for. More specifically, positive correlations between southward wind stress and increased pigment concentration occur in the 25 km next to the coast between 35°N and 47°N, but correlation coefficients are less than or equal to 0.3, accounting for

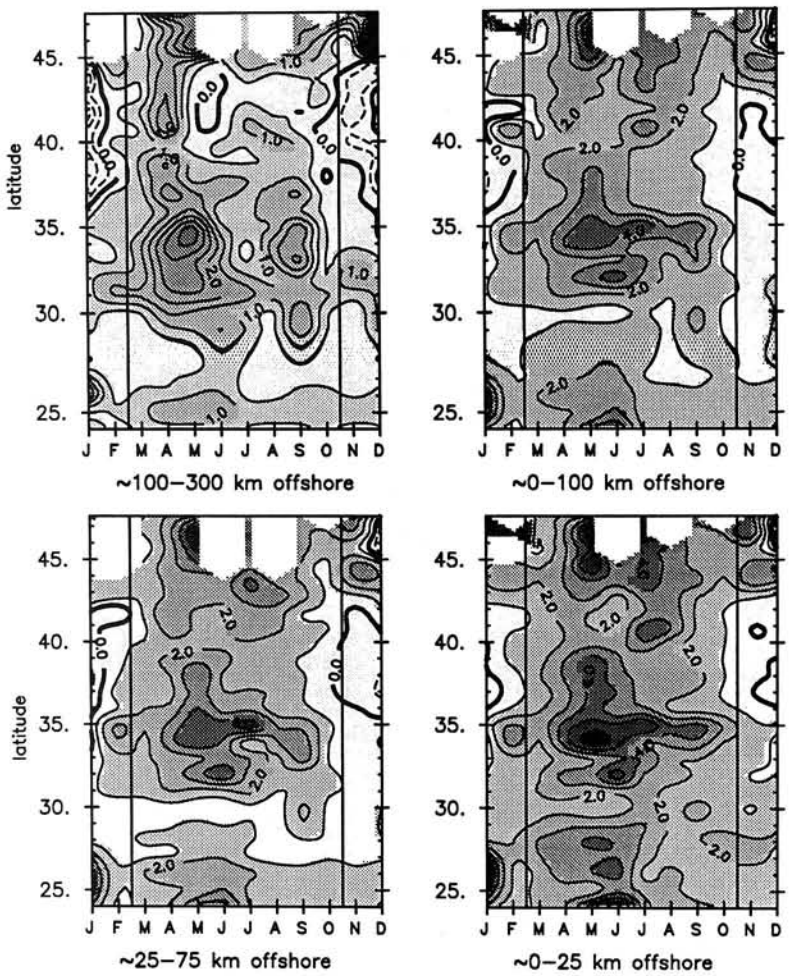

Fig. 4c. Seasonal cycles, as in Figure 4a, except formed from the corrected WCTS data set for the same 2-year period shown in Figure 4b.

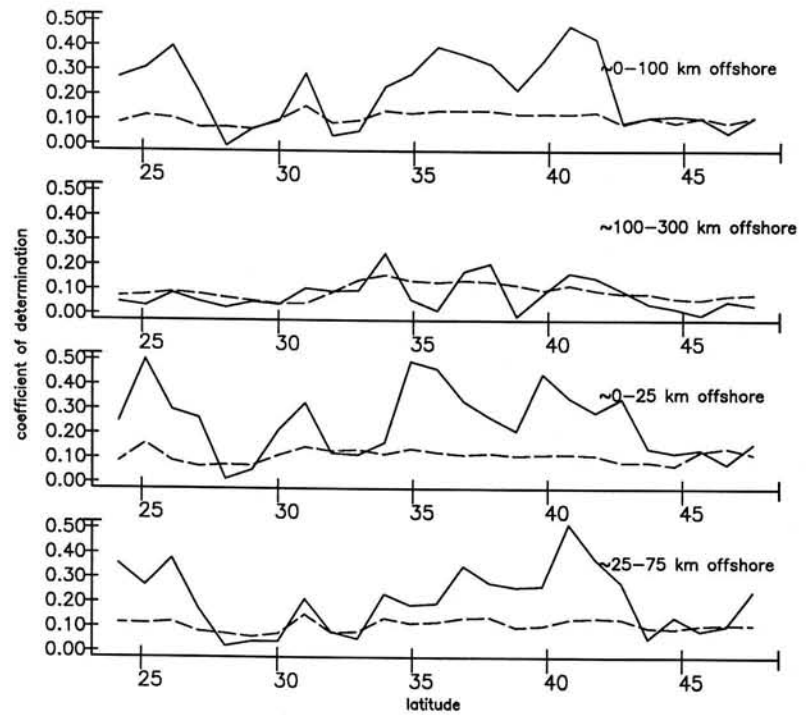

Fig. 4d. Coefficient of determination (fraction of variance explained) for fits of annual and semiannual harmonics to the data in the same bands as shown in Figure 4a. The dashed line gives the 95% significance level.

only 1–10% of the variance at a few locations. For the other wind variables, the highest point correlations are between pigment concentration and u_*^3 between 35°N and 46°N in the region 200–400 km from the coast, where the maximum value of r is 0.49 at 44°N (explaining 24% of the variance). Pigment concentrations are also correlated with wind stress curl between 34°N and 40°N in the 200 km region next to the coast (maximum $r = 0.40$, explaining 16% of the variance). Bootstrap estimates of the 95% confidence level for these correlations show that values of $r \approx 0.25$ are significant at the 95% level.

4.2.2. *EOFs of anomalous chlorophyll pigment concentration.* Figure 5 shows the first three EOFs of the monthly pigment concentration anomalies on the 1° blocks. Most of the variance occurs north of approximately 31°N, and comparisons with wind forcing in the next section are restricted to that region. The full EOFs are shown here for completeness. These three functions account for 34.5%, 11.3%, and 7.6% of the total pigment variance. The spatial functions resemble the typical geometric patterns described by *Richman* [1986], with no zero crossing in the first, a north-south separation in the second, and an east-west separation in the third. When the functions are recalculated using only data north of 31°N (these are the functions used in the subsequent PEP analysis) they explain more of the variance (39.0%, 12.4%, and 8.8%), and the only change is a shrinking of the regions where the first spatial function exceeds values of 1.5.

These three functions account for 60% of the interannual variability north of 31°N. The first function appears to be dominated by a low-frequency change from low values in 1979 to higher pigment concentrations in 1980–1982, followed by extremely low values beginning in April 1983, returning in 1985–1986 to moderately low values similar to 1979. Although relatively low concentrations continue to be found over the large-scale California Current in 1985 and 1986, values in the north (function 2) and in the narrower coastal region (function 3) are high again in spring 1986. This extends and quantifies the picture of low values of pigment concentration derived from CZCS data during the 1982–1983 El Niño previously described by *Fiedler* [1984] off southern California. The high values in the spring of 1986 and the similarity of values for the first function in 1979 and 1985–1986 provides support for the contention

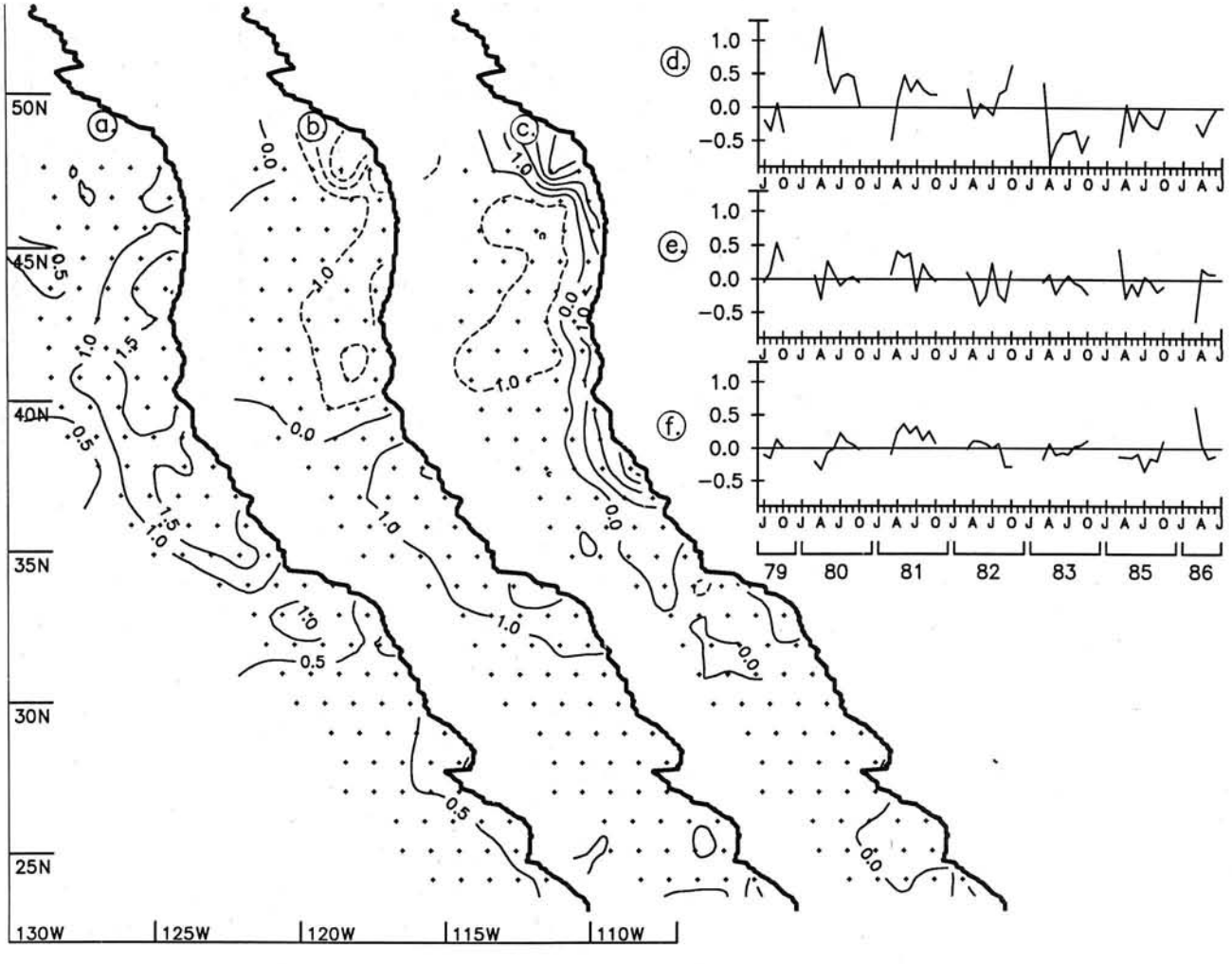

Fig. 5. The first three EOFs of monthly anomalous pigment variance from the data averaged to the grid in Figure 1. The product of space and time functions give anomalies in milligrams per cubic meter. The first three EOFs account for 34.7%, 11.3%, and 7.6% of the anomaly variance (respectively) over the domain shown here. Space functions for *(a)* EOF 1, *(b)* EOF 2, and *(c)* EOF 3; time series for *(d)* EOF 1, *(e)* EOF 2, and *(f)* EOF 3. Note that 1984 is omitted from the time series.

that the long-term trend in the decrease in sensitivity of the sensor has been adequately accounted for.

Changing spatial patterns of pigment concentration are described by combinations of these three functions. In the second half of 1979, the only strong function is the second, showing an increase in pigment concentration in the south in fall. In 1980 the dominant feature is the large-scale bloom (function 1) in spring, followed by the decrease in offshore concentrations and increasing coastal concentration (function 3) in midsummer. The third function is strong for most of 1981 and the first function is weaker than in 1980, reflecting the stronger confinement of the spring bloom and summer pigment concentrations to the coastal region. The second function indicates greater concentrations in the south in 1981 and greater concentrations in the north in 1982. This is consistent with previous observations of winds, currents and sea level in 1981–1982, which showed the spring transition and general upwelling region to be more confined to the north in 1982 than in 1981 [*Strub et al.*, 1987*b*]. The situation in 1982 is otherwise more confused until the end of summer, when pigment concentrations rise in the large-scale region (function 1). Beginning in April 1983 the dominant feature is the large-scale reduction of surface pigment concentration noted earlier. The only positive anomalies thereafter occur in the south in March 1985 (function 2) and in a northern, coastal band in March 1986 (functions 2 and 3).

4.2.3. *PEP analysis.* Table 1 shows the percent of total chlorophyll and wind variance accounted for by each PEP, the skill in predicting the first pigment EOF, and the chi-square significance level resulting from the PEP analyses, assuming 10 degrees of freedom (see Appendix B). Two domains are used for the pigment analysis. The wider region (Figure 1) composed of five 1° bands next to the coast from 31°N to 50°N is called the large-scale CCS region (left four columns in Table 1). A narrow region composed of four 0.28° bands (still 1° in latitude) from 31°N to 50°N is called the coastal band (right four columns in Table 1). Subdivision of the narrow nearshore region into these four bands of 0.28° (25 km) width is motivated by the assumption that the physical and biological response to wind-driven coastal upwelling should be strongest over the shelf, which has scales of 20–40 km in our region. Two domains are also used for the wind analysis. Wind fields on the original LFM grid, covering the large-scale two-dimensional CCS region, are referred to as "synoptic" (top three rows of Table 1). The area covered by these synoptic fields extends farther offshore than the 5° covered by the pigment data (Figure 6 shows the location of data variables). Wind variables interpolated to just the centers of the one-dimensional north-south band closest (0.5°) to shore in Figure 1 are referred to as "coastal" (bottom three rows of Table 1).

Over the large-scale CCS region, (Table 1, left), the synoptic wind variable that explains the most variance in the first PEP is the wind stress curl. The spatial functions for each variable and the common time series function are shown in Figure 6. The spatial functions show both offshore and coastal regions of maximum positive wind stress curl which correspond to positive coastal pigment concentration anomalies of up to 1.0 mg m^{-3}. This mode accounts for 62% of the first pigment EOF, $\approx$ 25% of total chlorophyll variance, and 8.5% of the large-scale curl variance. Both spatial functions have greater values in the southern region (35°N to 38°N). The overall pattern of the time series shows a long-term fluctuation, similar to that seen in the time series of the first pigment EOF (Figure 5*d*): high values in 1980–1981, a sudden drop in April 1983, and low values thereafter. The significance level based on 10 degrees of freedom is 95%. The higher PEP modes based on synoptic wind stress curl are much less significant. The first PEPs of the other two synoptic wind variables (u_*^3 and τ_y) explain less pigment variance and are less statistically significant (Table 1). The spatial fields of these wind variables (not shown) describe an offshore maximum in southward wind stress and u_*^3 over the location of the zero curl contour in Figure 6, rather than maxima over the chlorophyll maxima. These are the patterns which create the positive curl between the maximum southward stress and the coast. Thus they support the interpretation that wind stress curl is the synoptic field most closely correlated to large-scale anomalous chlorophyll.

Results of the PEP statistics comparing the large-scale pigment concentrations with wind variables confined to a coastal strip 0.5° from shore are shown in Table 1 (bottom left). The motivation is to see whether wind forcing adjacent to the coast (for instance, upwelling favorable winds) might result in higher concentrations, which are then advected offshore. The test was primarily designed for τ_a, which would cause both upwelling and offshore Ekman advection, rather than for wind stress curl or u_*^3, which should work in a local fashion. For all three wind variables, the skill (amount of large-scale pigment variance explained) goes down, although the statistical significance increases for u_*^3 and τ_a. The increase in significance is partly because the artificial skill is greater for the synoptic

TABLE 1. Principal Estimator Statistics

	5° Wide Band				Coastal Band			
	Pigment Variance, %	Wind Variance, %	Skill	χ^2 Significance	Pigment Variance, %	Wind Variance, %	Skill	χ^2 Significance
				Synoptic				
Curl τ	24.7	8.5	0.62	0.95	24.3	10.1	0.63	0.93
u_*^3	18.5	3.8	0.46	0.82	20.8	4.0	0.54	0.94
τ_y	15.7	7.0	0.37	0.73	19.7	5.9	0.50	0.90
				Coastal				
Curl τ	9.0	33.5	0.20	0.73	7.9	45.5	0.19	0.80
u_*^3	18.1	17.8	0.41	0.99+	22.8	16.6	0.56	0.99+
τ_a	13.7	12.5	0.29	0.92	19.3	11.5	0.47	0.99+

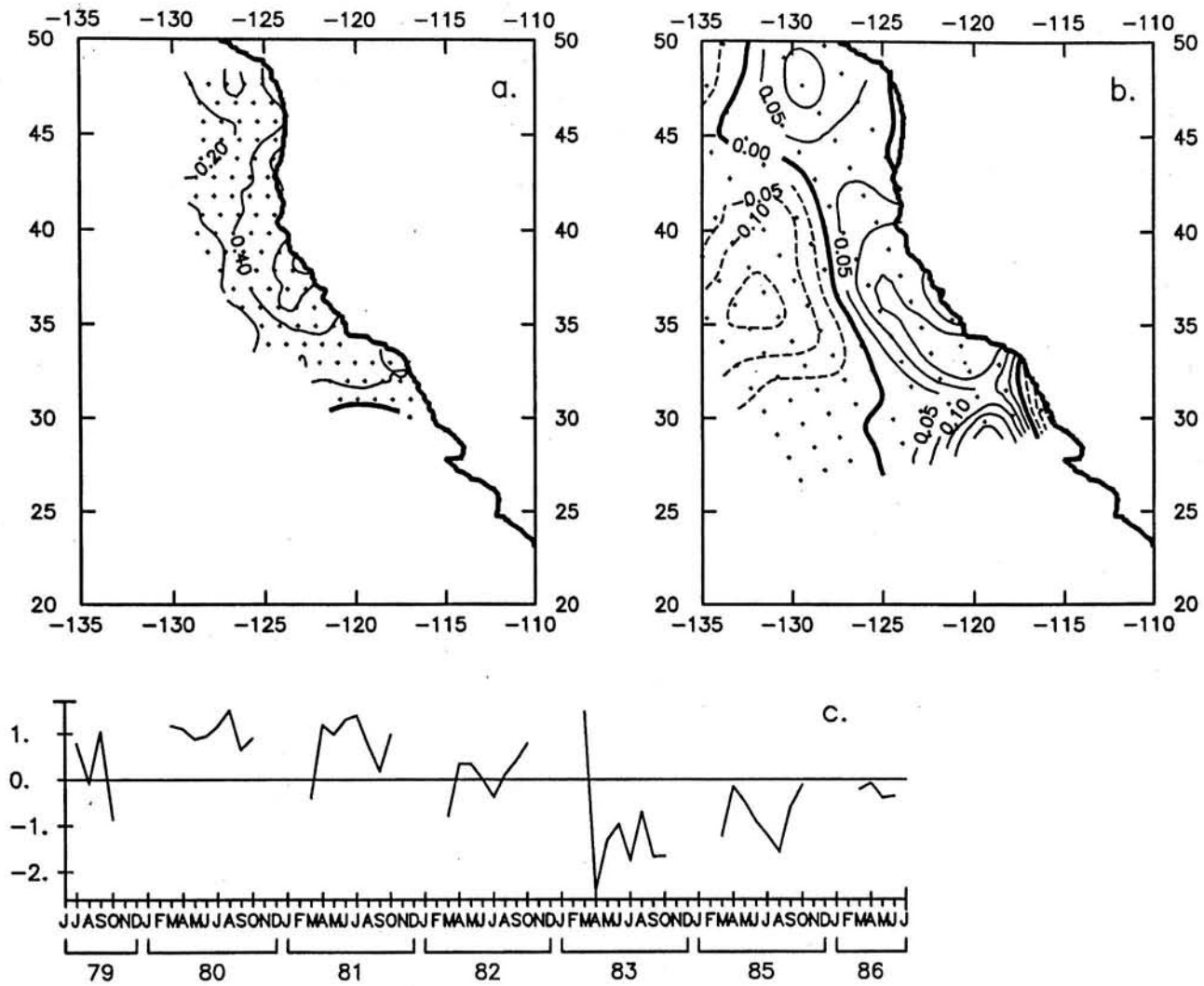

Fig. 6. The first spatial PEPs for *(a)* pigment in the large-scale CCS and *(b)* synoptic curl τ, and *(c)* the common time series for both. Units for the product of space and time functions are milligrams per cubic meter and (10^{-7} N m^{-3}). The grid for each variable is indicated by dots.

wind fields than for the coastal strip (you can explain more chlorophyll variance by regressing against random winds at many points than at fewer points). Thus the chi-square statistics (ratios of variance explained to artificial skill) are larger for the coastal wind than for the synoptic wind fields. One can argue that the high significance level for u_*^3 in the coastal band is physically reasonable, since increased mixing power would be more effective in enriching the surface layer in the 100 km next to the coast, where the nutricline is closer to the surface owing to upwelling.

The greater importance of u_*^3 and τ_a next to the coast is supported by the fact that these become the wind variables most closely related to pigment concentration when wind variables and pigment concentrations are all restricted to the 100 km next to the coast. Results of the PEP analysis confined to this coastal band are presented in Table 1 (bottom right). The relation between pigment and wind stress curl is not significant, and only u_*^3 and τ_a explain a significant amount of variance (23% and 19%, respectively). The first PEP spatial and temporal patterns for this coastal analysis are shown for u_*^3 and τ_a in Figures 7 and 8, respectively. The spatial patterns for pigment concentration are similar, with greater values next to the coast, although the pigment maxima are located in different regions. Pigment maxima associated with u_*^3 occur between Point Arena and Cape Mendocino and north of Cape Blanco, while those associated with higher τ_a are located around Monterey Bay and between capes Mendocino and Blanco. The spatial function of u_*^3 is positive north of 37°N and becomes very negative to the south (Figure 7). The spatial function for alongshore wind stress is northward south of 37°N, southward between 37°N and 43°N, and northward north of 43°N (Figure 8). Since winds are southward (on average) in the south and the absolute magnitude of u_*^3 cannot be negative, we interpret positive values of the time series to indicate anomalously weak southward winds (or northward winds) south of 37°N and stronger southward winds between 37°N and 43°N, caused by a shift in the position and/or strength of the high pressure system next to the coast. The region of stronger winds between 35°N and 43°N coincides with the region of greatest increase in pigment concentration.

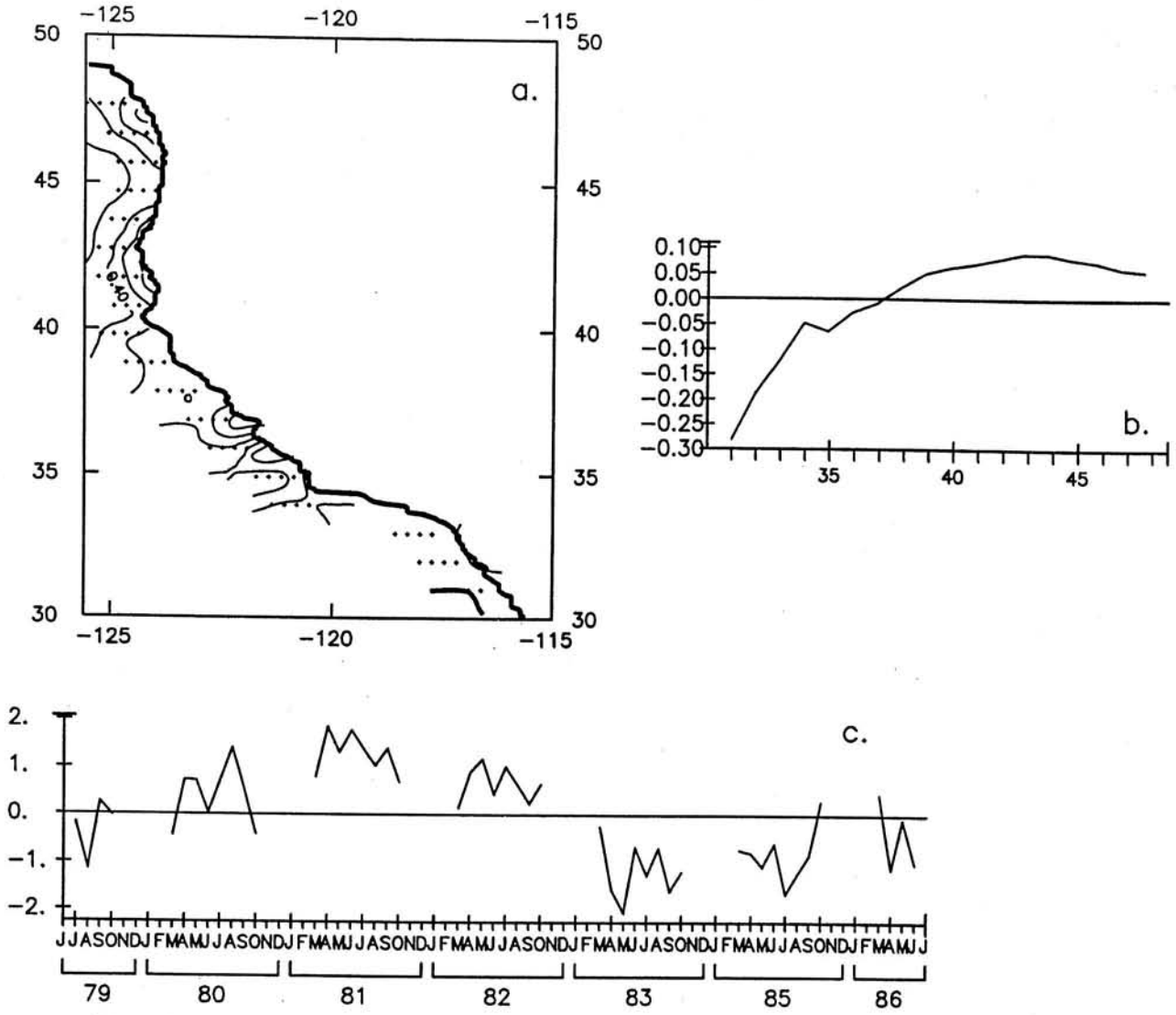

Fig. 7. As in Figure 6 for *(a)* pigment in the narrow coastal strip (four 0.28° wide bands) and *(b)* u_*^3 at locations 0.5° from the coast centered on the pigment grid, and *(c)* the common time series for both. Units for u_*^3 are (10^{-6} m^3 s^{-3}). Note the expansion of the horizontal scale in Figure 7*a*.

When the narrow band of coastal pigment is compared with the large-scale synoptic wind fields, all are significant at the 90–94% level and account for ≈ 20–24% of the anomalous coastal pigment variance (Table 1, top right). The spatial functions are very similar to those found before, with maximum u_*^3 and southward wind stress in a region ≈ 400 km offshore over the line of zero wind stress curl. The curl is positive in the 400 km next to the coast with maximum values both ≈ 200 km offshore and next to the coast as in Figure 7. Thus as before, all three fields argue for the importance of synoptic wind stress curl. In this case, however, the lack of correlation between pigment in the coastal band and wind stress curl immediately over it (Table 1, bottom right) weakens the argument for the importance of wind stress curl in the 100 km next to the coast, unless its spatial distribution near the coast is poorly represented by the LFM fields (a distinct possibility).

The process of identifying the most important of the wind variables is complicated by the high correlation that exists between τ_a, u_*^3, and large-scale curl, making the separation of their effects difficult. There is also a close tie between the physical effects of the three wind variables, since higher levels of surface mixing (u_*^3) will be more effective in bringing nutrients into the surface layer in the presence of upwelling (caused by either τ_a or wind stress curl). Our interpretation of these statistics is that anomalous synoptic wind stress curl is the important variable for the large-scale changes in anomalous pigment; in the region closer to the coast, the evidence is less supportive of wind stress curl and favors u_*^3 and τ_a, but cannot differentiate between them.

5. Discussion

5.1. *The Seasonal Cycle*

Due to the use of the correction function, the seasonal cycles presented in Figure 4*a* must be viewed as the signal that remains after removing the component of the north-south gradient with an annual peak in winter (Figure 2*a*). The temporal amplitude of the correction is ≤ 0.1 in June–

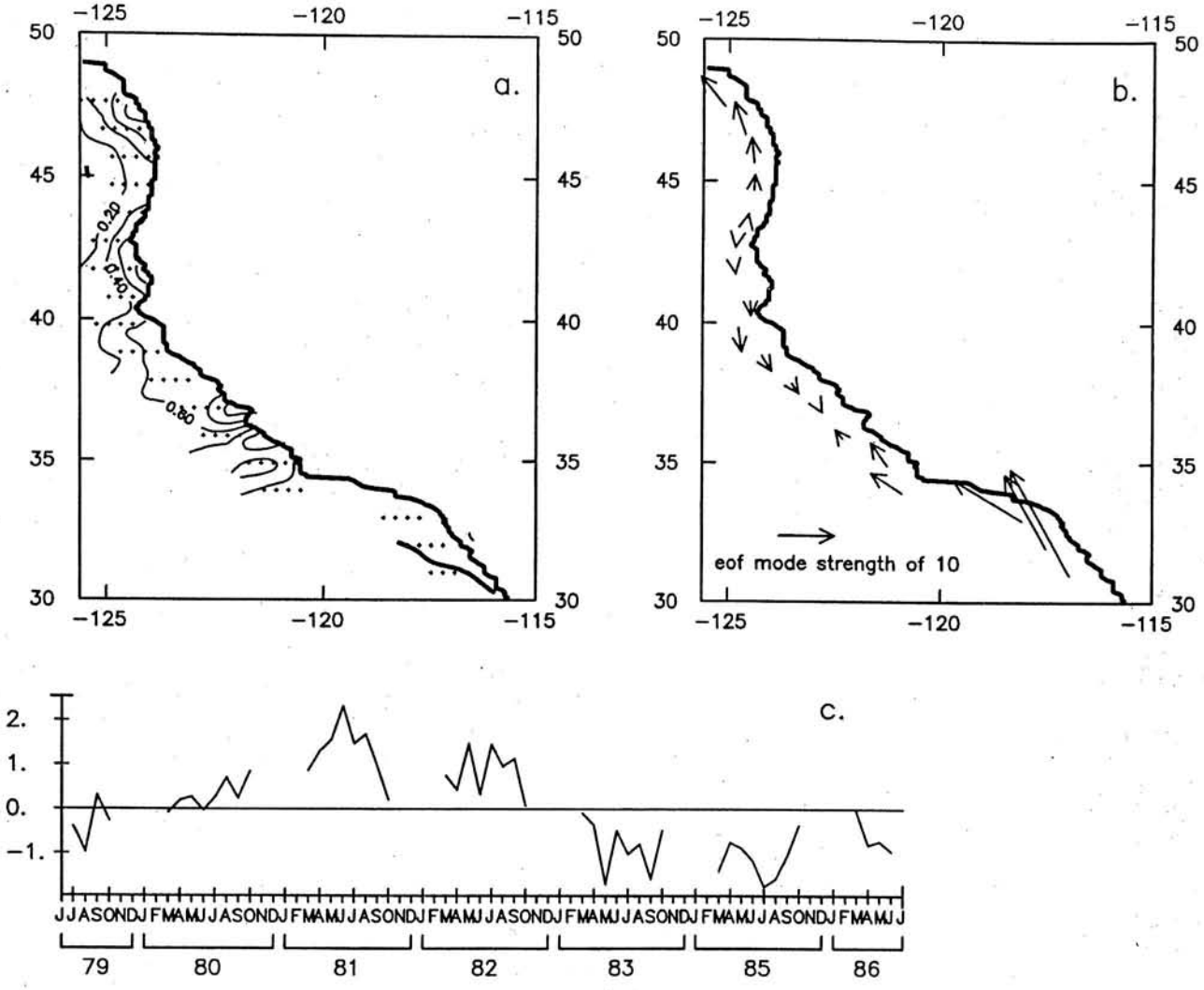

Fig. 8. As in Figure 7 for (*a*) pigment in the narrow coastal strip, and (*b*) alongshore wind stress 0.5° from the coast, and (*c*) the common time series. Units for wind stress are (10^{-3} N m^{-2}).

August (virtually nothing is subtracted at any latitude in those months) and ≈ 2.7 in January. The spatial amplitude is zero at 24°N (nothing is subtracted in any month at that latitude) and is ≈ 1.5 at 48°N. In the March–October period the maximum correction is at 48°N in October, with a value of ≈ 1.2 mg m^{-3}.

In the Southern California Bight between 29°N and 33°N, the primary conclusion from the analysis presented here is that seasonality is very low. The primary seasonal feature identifiable in the March–October period is the late summer minimum in the region 25–100 km from the coast in Figure 4*a* (most clearly seen in the bottom left and top right panels). Since the correction function removes less than 0.3 mg m^{-3} south of 33°N, we would argue that this summer minimum is not caused by our correction function. The low seasonality and the summer minimum are qualitatively in agreement with results from *Eppley et al.* [1985] from in situ data. Thus the March–October seasonal cycle in the corrected surface pigment concentration appears qualitatively in agreement with in situ studies of the southern region. In the northern portion of the study area, the CZCS climatology is in good agreement with that of *Landry et al.* [1989], even though the correction function is large in winter. In particular the double peak (spring and summer) reported off Washington by Landry et al. is present within 25 km of the coast in Figure 4*a* (bottom right). This degree of agreement between seasonal cycles derived from the corrected WCTS CZCS and historical in situ pigment concentrations in a southern and a northern region gives us some confidence in the patterns presented in Figures 2*c* and 4*a* and in Plate 1. The spatially locked pattern in Figure 2*c* accounts for 36% of the variance in the corrected data; fits of annual and semiannual harmonics result in seasonal cycles similar to Figure 4*a* that account for a similar amount of variance (30%–50%) in the region between 33°N and 43°N within 100 km of the coast.

Plate 1 and Figure 4*a* show that the lack of a spring bloom off Oregon suggested by the few data available to Landry et al. appears to be real, at least for the 1979–1986 mean. It should be noted, however, that there is a large degree of interannual variability in the satellite-derived pigment concentration at the time of spring transition [*Thomas and Strub*, 1989] and a spring bloom does appear

off Oregon in some years, in particular, 1980 and 1982 of the present data set. Thus Figures 4*b* and 4*c* show higher spring values in the region within 25 km of the coast off Oregon in these 2-year means.

The northward migration of high pigment values from northern California to Oregon between May and August, evident in Figures 4*a* to 4*c*, is consistent with the appearance of offshore filaments of pigment in the northern part of the CCS in individual CZCS images from late summer and fall and with the seasonal northward migration of maximum southward wind stress [*Strub et al.*, 1987*a*]. The narrow meandering region of high pigment concentration off northern California in summer (Plate 1) has been investigated in detail during summer 1987 and 1988 during the Coastal Transition Zone experiment (CTZ) [*CTZ Group*, 1988]. Results indicate that a meandering surface jet forms the offshore boundary of the high pigment concentration region, causing its scalloped appearance. The maximum seen west of San Francisco may be exaggerated by the presence of case II water from San Francisco Bay; this is also a region where filaments originating at Cape Mendocino and Point Arena carry both pigment and gelbstoffe offshore, making the interpretation of the CZCS signal more difficult.

The low seasonality and low surface pigment concentrations in the Southern California Bight have been well documented and attributed to the onshore flow of oligotrophic offshore water [*Peláez and McGowan*, 1986]. The same authors note the higher productivity around the Channel Islands, as do *Smith et al.* [1988]. As was described above, *Michaelsen et al.* [1988] present seasonal cycles from $\approx$ 31°N to 36°N that have an inverted seasonal cycle (winter maximum, summer minimum). They attribute the summer minimum to the sensor's inability to see the deep chlorophyll maximum which develops under the highly stratified and nutrient depleted surface layer. Although we would suggest that much of the winter maximum in their cycle omes from errors in the atmospheric scattering algorithm, we are in agreement with the finding of a late summer minimum between 31°N and 34°N, although this is a minor effect. The summer minimum is consistent with the climatological monthly geostrophic velocity fields derived from California Cooperative Oceanic Fisheries Investigations (CalCOFI) data [*Roesler and Chelton*, 1987], which show stronger onshore flow into the bight in summer, pushing this oligotrophic water both southward and northward. The same monthly fields show that in September an alongshore northward current develops next to the coast north of Punta Eugenia that may bring more eutrophic water into the bight from the upwelling region off Baja California, ending the summer minimum. Off Baja California, higher pigment concentrations in summer are similar in magnitude and timing to those off central and northern California. This clarifies the fact that the low concentrations in the eastward flowing current entering the bight are more of an intrusion over the California Current rather than the southern end of the productive region, especially in the 100 km next to the coast (Figure 4*a*).

An alternate suggestion concerning the summer minimum in the bight is that it is an artifact of a seasonal change in the aerosols over the bight, caused by the incorrect assumption of uniform marine aerosols in the image processing. Only a detailed reprocessing of the data can determine whether a systematic error is caused by the assumption of uniform aerosols. Given the consistency of the summer minimum with previous in situ measurements [*Eppley et al.*, 1985] and with the seasonal changes in the geostrophic currents noted above, we favor the view that it is a real, although minor, phenomenon. We emphasize, however, that the primary conclusion concerning the Southern California Bight is that it is a region of very low seasonality in comparison to the rest of the California Current. Conclusions based on data from this anomalous region should not be used to characterize the CCS.

Seasonal cycles of the wind variables in the coastal band (0.5° from the coast), calculated for the same period as the pigment data, are presented in Figure 9 for comparison with Figure 4*a*. There is a good visual correspondence between the seasonal cycles of pigment concentration in the coastal bands of Figure 4*a* and both upwelling favorable wind stress and wind stress curl in Figure 9 north of 35°N. The slope of the northward progression of higher pigment concentrations in March to July at these latitudes is similar to that of negative (southward) alongshore wind stress. Correspondence is especially strong between the summer maxima of pigment concentration, southward wind stress, and positive curl between 35°N and 40°N and between spring and fall minima in pigment concentration and negative wind stress curl between 40°N and 45°N. Comparison of these curl data to climatological curl fields [*Nelson*, 1977] leads us to question the lack of a positive curl in the coastal region off Oregon in the summer in Figure 9. If one connects the regions of positive curl south

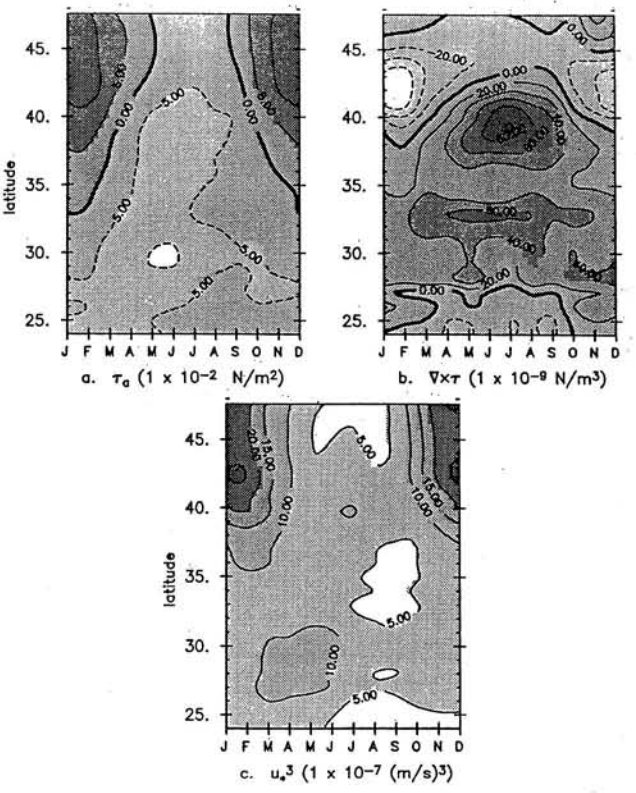

Fig. 9. Seasonal cycles of *(a)* alongshore wind stress (10^{-2} N m^{-2}), *(b)* curl τ (10^{-9} N m^{-3}), and *(c)* u_*^3 (10^{-7} m^3 s^{-3}), in the coastal band, contoured as in Figure 4*a*.

of 43°N and north of 46°N, a northward progression in time is seen, similar to those of pigment maxima and southward windstress. There is also a strong seasonal pattern in u_*^3 north of 35°N, reaching a minimum in mid to late summer. Between 26°N and 31°N this pattern is reversed and has a much lower amplitude, with a maximum in spring. The region where this seasonal pattern may influence pigment concentrations most is in the north, where one expects winter mixed layer depths and surface nutrient levels to be greater. The onset of a spring bloom at these latitudes may take place under conditions similar to those of the North Atlantic, where net positive phytoplankton productivity begins as the mixing power of the wind decreases and light and stratification increase [*Sverdrup*, 1953; *Riley*, 1957]. A North Atlantic type spring bloom does not usually occur off northern and central California [*Thomas and Strub*, 1989], where the upper water column appears nutrient limited even in late winter. Calculation of correlations between the seasonal cycles of pigment and wind result in high values in the regions where the variables covary most strongly, but no statistical certainty can be calculated for these correlations owing to the low number of degrees of freedom in the seasonal cycles and the tendency for all seasonal cycles to correlate artificially well [*Chelton*, 1982*b*].

5.2. *Nonseasonal Variability*

Much of the large-scale nonseasonal variance of anomalous pigment concentration appears as a single long-period oscillation centered around the 1982–1983 El Niño (EOF 1 in Figure 5). Wind variables would need to have much of their nonseasonal variance in a similar oscillation to yield significant correlations between the raw time series at a given location, which is usually not the case. The PEP method finds that part of the variance of the anomalous wind that covaries with the pigment anomalies.

5.2.1. *Relation to wind variables.* Over the 5° wide CCS region, the wind variable that covaries with the anomalous pigment concentration most strongly is the wind stress curl. The first PEP describes a band of positive curl 400 km wide with a maximum located ≈ 200 km offshore and anomalously high pigment concentrations over the entire CCS, with maximum values at 38°N near the coast (Figure 6). Approximately 25% of the total variance of anomalous pigment concentration and 8.5% of anomalous curl variance are contained in this function. Although this may seem like a small amount of pigment variance (corresponding to an equivalent correlation coefficient of $r = 0.5$), much of the total pigment variance in the satellite data may be noise, caused by the various sources of error described in section 3 and Appendix A, and actual small-scale variance related to local biological and physical factors, which are not adequately resolved in space and time in our analysis. The LFM winds also fail to accurately represent wind variance with spatial scales less than approximately 600 km. Assuming that the first pigment EOF is the important large-scale signal, the ability to explain 62% of its variance (Table 1) is the significant result. The other synoptic wind fields examined explain lower amounts of the pigment and wind variance in the large-scale CCS. More importantly, they have the spatial functions consistent with positive wind stress curl.

Values of the spatial and temporal functions result in peak pigment anomalies of ± 1.5 mg m^{-3} and peak curl anomalies of 4×10^{-8} N m^{-3}. Our comparisons of the LFM winds used here with buoy winds show that while spatial differences (such as those used in the curl calculation) are coherent, the LFM fields underestimate the magnitudes of the measured horizontal differences by a factor of approximately 5–10 [*Strub and James*, 1990]. Maximum curl anomalies are therefore likely to be of the order of 2–4 $\times 10^{-7}$ N m^{-3}. These values would lead, through Ekman pumping, to vertical displacements of ≈ 5–10 m per month, enough to have an effect on the normally shallow (20–40 m) pycnoclines found in summer and potentially contribute to nutrient flux into the euphotic zone.

When the wind variables and pigment concentrations are confined to the 100-km-wide coastal strip, the significant correlations explaining the greatest amount of pigment variance are found for u_*^3 and alongshore wind stress, accounting for 56% and 47% of the first pigment EOF, respectively. It is difficult to separate the effects of wind mixing (u_*^3) from upwelling (τ_a) in the present data. The spatial functions of wind variables suggest shifts in strength and position of the atmospheric high pressure system off northern California, leading to both greater upwelling and wind mixing. Our analysis cannot differentiate between the two processes, which are highly correlated with each other.

The correspondence between anomalous large-scale pigment concentration and wind stress curl over the CCS is similar to the relation between anomalous curl, southward transport, and zooplankton volume found by *Chelton* [1982*a*] and *Chelton et al.* [1982] from CalCOFI data off central and southern California. In the narrower region within 100 km of the coast, the correspondence between anomalous pigment concentration and alongshore wind stress and/or u_*^3 is more like the expected relation between an upwelling index (alongshore wind stress divided by Coriolis parameter) and biological response [*Bakun*, 1973]. Off Oregon and Washington, *Landry et al.* [1989] find correlations of ≈ 0.35 between the upwelling index and surface chlorophyll based on limited field data and correlations of 0.3–0.5 between the upwelling index and in situ nutrient data. These values are similar to the highest point correlations found here between alongshore wind stress and pigment ($r \leq 0.3$) and the amount of pigment variance explained in the coastal band by the PEP of alongshore wind stress (≈ 20%, which would correspond to an equivalent $r = 0.45$). As in the wider, 5° region, the fact that the wind variables explain ≈ 50% of the first pigment EOF is the significant finding.

5.2.2. *Relation to the El Niño.* Previous studies show the physical manifestations of the 1982–1983 El Niño in the CCS to cover the period between November 1982 and mid-1984. High SST and sea level appeared in November 1982 and were maximum by 2 standard deviations over most of the CCS in winter 1982–1983 [*Norton et al.*, 1985; *Strub et al.*, 1987*a*]. High temperatures and low salinities were seen over most of the CCS in 1983, but by the end of 1984, *Rienecker and Mooers* [1986] show the subsurface water characteristics off central and northern California to be only slightly warm (1 standard deviation) and salty, rather than fresh. Off central California, *Chelton et al.* [1988] document warm, salty water flowing northward in July

1984, as opposed to the warm, fresh water found in August 1983 by *Simpson* [1984]. By January 1985, temperature and salinity off central California were more or less normal in a strongly northward flowing Davidson Current [*Chelton and Kosro*, 1987]. Off central Oregon, sea level and SST returned to normal values by the end of 1984 [*Huyer and Smith*, 1985].

Biologically, a northward displacement of a large number of species was observed in 1983 [*Miller et al.*, 1985; *Pearcy and Schoener*, 1987]. Both satellite [*Fiedler*, 1984] and in situ data [*McGowan*, 1985] show that phytoplankton pigment concentrations off southern California were anomalously low by March 1983. McGowan found the nutricline in the Southern California Bight to have deepened from its normal depth of 50 m to 80 m in March 1983. Phytoplankton response to the El Niño was maximum in late summer and fall, lagging behind the physical anomalies but then responding rapidly. McGowan states that one of the most distinct features of the phytoplankton distribution during this period was the disappearance of the region of maximum surface biomass in the offshore area of the Southern California Bight, south of Point Conception. Off Oregon, surface chlorophyll values in June 1983 were below 1.0 mg m^{-3} in the 25 km next to the coast, in comparison to normal values greater than 3 mg m^{-3}; concentrations were higher off Washington but still below normal [*Pearcy et al.*, 1985]. In September 1983, chlorophyll concentrations of 3–8 mg m^{-3} were found north of 45°N, but concentrations dropped to less than 1 mg m^{-3} south of 44°N [*Fisher et al.*, 1984]. Similar patterns of low values off southern Oregon and higher values off northern Oregon and Washington were found in September 1984 and June 1985 [*Fisher and Pearcy*, 1985*a*, *b*].

The time series of the first EOF of pigment concentrations (Figure 5*d*) gives the appearance of relatively low values extending into 1985 and 1986. Time-latitude contours of the monthly anomaly data from the same longitudinal bands used in Figure 4*a* (not shown) give a similar impression but show that the pigment values were not as low after August 1983 north of the Columbia River and that slightly positive anomalies reappear in a patchy pattern over most of the domain in 1985 and 1986.

The clearest presentation of the nature of the differences in the fields before and after the El Niño comes from a comparison of selected spring and fall individual monthly composites from fall 1979 to spring 1986 (Plate 2). Neither the mean seasonal cycle nor the empirical correction function has been subtracted from these monthly means, since the purpose of the figure is to allow a comparison of similar months on different years. These may be placed in the context of the time series in Figure 5*d*. The monthly mean from October 1979 shows the fall pattern during the period of relatively low pigment concentration early in the time series. April and September 1981 present spring and fall patterns in a year with moderately high pigment concentrations. Similar pictures can be found in 1980 and 1982 (not shown). These can be compared with the very low values following the El Niño in April and September 1983, where high pigment concentrations are restricted to very narrow coastal regions south of some latitude. Higher values existed farther from shore north of 43°N in April 1983 and north of 40°N in September 1983. October 1983 (not shown) was similar to September 1983. Higher pigment concentrations are present in September 1984 north of 36°N (Plate 2), although this northern region is still narrower and lower in concentration than September 1981. In September 1985, the broad pigment front has moved back north to ≈ 40°N. In August of 1984 and 1985 (not shown), the broad front was lacking and the pattern consisted of a narrow coastal band of high pigment concentration stretching north from Point Conception (35°N), similar to the pattern south of 40°N in September 1985. In October 1985 (not shown) the pattern is similar to September 1985 except that the front has moved south to 36°N. Pigment concentrations in April 1986 are similar in pattern to 1981, but remain lower in concentration. Thus the patterns found from April 1983 to sometime in 1986 are characterized by a narrow coastal band of high pigment concentration south of some latitude, as described off southern California during the El Niño by *Fiedler* [1984] and (during some months) by a wider region of high pigment concentration north of that latitude. The broad north-south gradient of pigment concentration separating these regions is similar to the pigment front found in the Southern California Bight in 1979–1982 [*Peláez and McGowan*, 1986]. By spring 1986, the front has return to its normal location, but values are still low in comparison to 1980–1982.

The low concentrations during 1983 and the north-south gradient off Oregon and Washington in 1984–1985, evident in the satellite data, agree with the few in situ data available, as reviewed above. This pattern may be related to the northward flow found off Oregon in 1983 [*Huyer and Smith*, 1985] and off central California in July 1984 and January 1985 [*Chelton et al.*, 1988; *Chelton and Kosro*, 1987]. Replacement of the warm, fresh water observed in 1983 with warm, salty and nutrient-poor water from the south would result in continued low primary productivity south of the northward extent of the advection, as seen in September 1984 and 1985 (Plate 2).

If the alongshore transport associated with the 1982–1983 El Niño were the dominant cause of interannual variability in the large-scale pigment concentration of the CCS, a strong relation should exist between pigment concentration and the strength of the transport in the California Current. Although no regular time series of the large-scale transport exists, coastal sea level serves as a proxy for the alongshore current over the shelf. Monthly mean sea levels from Newport and Coos Bay, Oregon (45°N and 43°N), have been obtained and adjusted for atmospheric pressure to form a time series of adjusted sea level (ASL). Correlations of nonseasonal anomalies of these time series to the time series from the first EOF of anomalous pigment concentration in both the 5° and 1.12° bands result in correlation coefficients of the right sign (negative) but marginally significant at best ($r \approx -0.25$). Correlations of the ASL anomalies to the anomalous pigment concentrations located immediately offshore of the sea level stations yield identical results. Thus the hypothesis that alongshore transport over the shelf, as represented by ASL, controls more of the variance in pigment concentration than local or large-scale wind forcing is not supported by this data. We do not argue, however, that the fields of pigment concentration in Plate 2

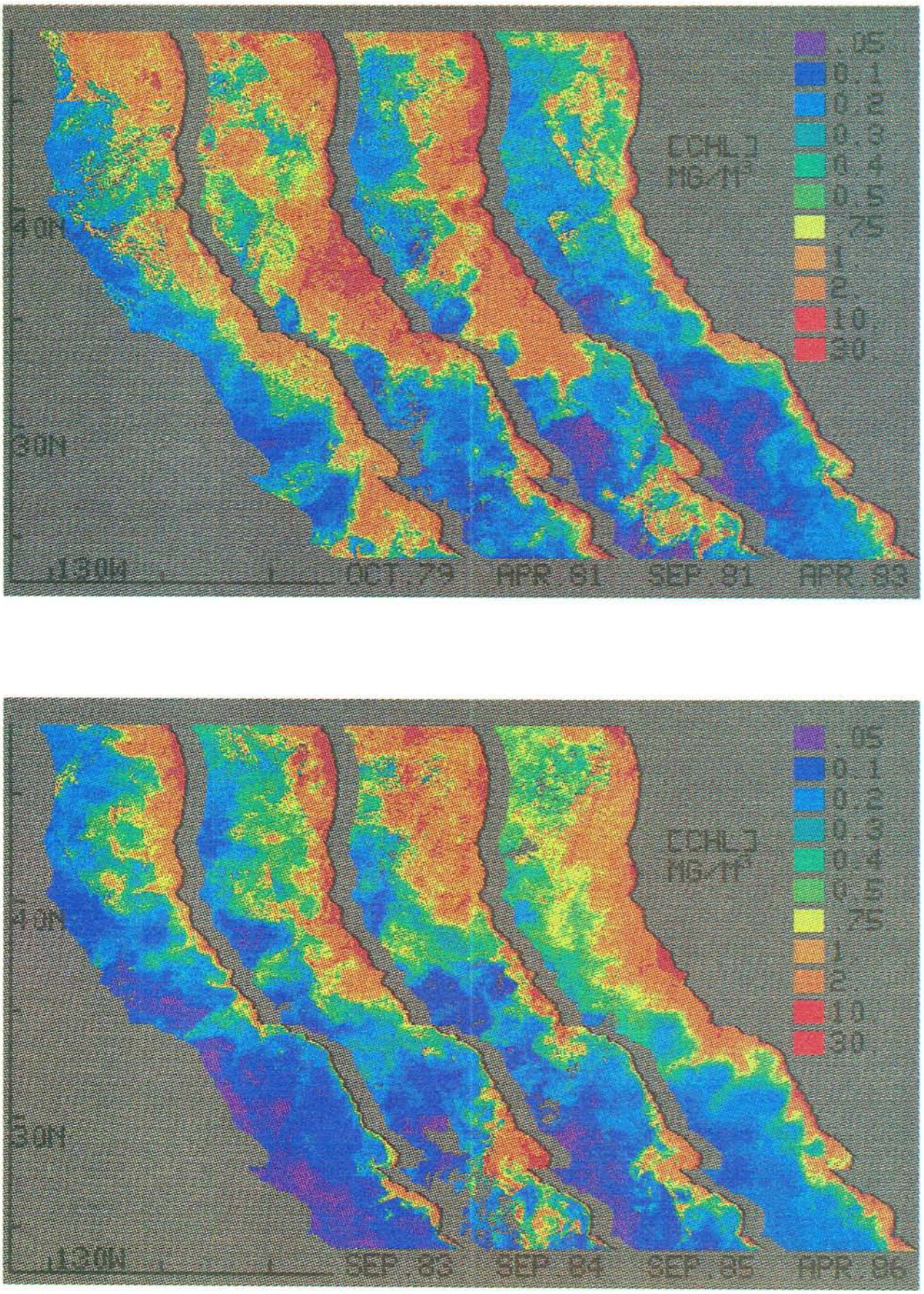

Plate 2. Monthly mean pigment concentrations for selected individual months, identified in each image. Neither the seasonal cycle nor the empirical correction function has been subtracted. Units are milligrams per cubic meter.

are unrelated to the true large-scale circulation of the CCS. On the contrary, the fluctuating alongshore displacement of the broad north-south gradient of pigment from its usual position off southern California suggests that the large-scale circulation was directly involved in creating this pattern, since the location of this pigment front is thought to be directly related to the onshore transport in the CCS [*Peláez and McGowan*, 1986]. Only when satellites yield quasi-coincident fields of satellite-derived surface pigment concentration and currents will we be able to investigate the direct connection between the two.

One is left with the picture of a slow oscillation in anomalous pigment concentration in the large-scale CCS that is related most strongly to a specific pattern of wind stress curl over the CCS. Only a small part of the variance of the curl field is represented by this pattern. There is also a relation to changes in water mass coincident with the El Niño, but the biological response appears more complex than indicators of coastal alongshore advection in the CCS such as ASL. The relation between fields of pigment concentration and the true large-scale circulation in the CCS remains unknown. Relatively long period variability has been found in the CCS by others in both physical variables such as surface temperature [*Norton et al.*, 1985] and biological variables such as crab catch [*Botsford*, 1986]. Although some of this variability can be explained statistically by wind stress curl or alongshore wind stress, a significant portion remains unexplained. Biological variability is inherently greater than the variability of any single physical factor in the surrounding environment, and responses are usually nonlinear, further increasing the difficulty of finding linear statistical relationships. The existence of long-period fluctuations such as seen here in anomalous pigment concentrations underscores the need for time series long enough to define the true variability of both the biological data and the physical environment.

6. Summary and Conclusions

6.1. *The Seasonal Cycle*

1. Use of the WCTS, corrected empirically for errors in the atmospheric algorithm, yields a reasonable March-October seasonal cycle of pigment concentration (Figures 2*c* and 4*a* and Plate 1): there is a spring bloom off Washington in April–May, with decreasing concentrations in June and increasing concentrations again in July; there is a seasonal increase off northern California in March–April, progressing northward to appear off Oregon in July; in the Southern California Bight, seasonality is low, with a relative minimum in late summer; off Baja California there is generally a maximum in summer, as off northern California, and a minimum in late summer, as in the bight. The most robust of these features are the low seasonality of the bight, the high degree of seasonality elsewhere, and the early maximum off Washington and central and northern California, progressing to the north off Oregon. There is more year-to-year variability in the appearance of the double maximum off Washington, the lack of the spring bloom off Oregon, and the late summer minimum in the bight.

2. Between 35°N and 45°N, summer patterns (Plate 1 and Figure 4*a*) show a relatively narrow region of high pigment concentration, with a scalloped nature. The region of pigment concentration may lie inshore of the southward jet in the CCS; in spring and fall the pattern is wider and more diffuse.

3. North of 35°N there is a good visual correspondence between the seasonal patterns of upwelling favorable winds, wind stress curl and pigment concentration (Figures 4*a* and 9).

6.2. *Nonseasonal Local Variability*

4. Point correlations between anomalous alongshore (upwelling favorable) wind stress and pigment concentration are only marginally significant ($r \leq 0.3$) in the 25 km next to the coast between 35°N and 45°N and insignificant elsewhere. Higher point correlations are found between anomalous pigment concentration and wind stress curl ($r \approx 0.4$) in the 200 km next to the coast from 35°N to 40°N and 300 km offshore at 46°N. The highest point correlations are found between anomalous pigment concentrations and u_*^3 in the region 200–400 km offshore between 35°N to 45°N ($r \approx 0.5$).

6.3. *Nonseasonal Large-Scale Variability*

5. The first EOF of anomalous pigment concentration (Figure 5) describes a coherent rise and fall of pigment concentrations in the CCS (accounting for 40% of the total pigment variance). The large-scale decrease in pigment concentration is centered on the 1982–1983 El Niño, but the overall time series (Figure 5*d*) has a longer period than the El Niño, approximately covering the 7 years of data.

6. PEP analysis reveals that this first pigment EOF is significantly correlated with the wind stress curl in a 400-km band next to the coast which has a maximum 200 km offshore between 35°N and 40°N; this PEP accounts for 62% of this pigment EOF (25% of the total variance of the anomalous pigment concentration) but only 8.5% of the total variance of the anomalous wind stress curl (Figure 6).

6.4. *Nonseasonal Coastal Variability*

7. In the 100 km next to the coast, the first pigment EOF is most closely related to u_*^3 (the first PEP explains 56% of the pigment EOF and 17% of the wind variance (Figure 7)) and alongshore wind stress (explaining 47% of the pigment EOF and 12% of the wind stress (Figure 8)). Both processes may act together to increase nutrients in the mixed layer.

6.5. *Interannual Variability and El Niño*

8. Although the 1982–1983 El Niño had a strong effect on the large-scale pigment values, the fluctuations in pigment concentration in some regions had a longer period than the El Niño. Correlation of pigment concentrations with proxies of coastal circulation such as sea level are usually less significant than those with local alongshore wind stress. A relation between the pigment concentration and the larger-scale circulation in the CCS is hinted at by individual monthly fields (Plate 2) but details remain unknown because of a lack of knowledge of monthly fields of transport. The long-period fluctuation described by the first EOF of anomalous pigment concentration (Figure 5*d*) is similar in nature to other long-period biological fluctuations in the CCS documented in the literature.

APPENDIX A: WEST COAST TIME SERIES

A1. *Methods of CZCS Processing*

The purpose of producing the west coast time series of CZCS data was to provide users with a consistently processed series of satellite-derived surface pigment fields in a timely fashion. The bulk of the level 1 (raw, sensor unit data) tapes were obtained from the Scripps Satellite Oceanography Facility along with a few calibrated radiance temperature (CRT) tapes from NOAA National Environmental Satellite Data and Information Service (NESDIS). Eight hundred thirteen tapes were copies from SSOF and 46 were acquired from NESDIS. These 813 tapes represented the entire holdings of level 1 CZCS data from the west coast at SSOF. Of the total 859 tapes, 22 were essentially duplicates between the SSOF and CRT tapes, 4 tapes had fatal tape recorder errors (extra lines, etc.), and 13 tapes had unreadable pass times. Of the remaining 820 tapes, 43 had no landmarks and thus could not be navigated and 5 had severe noise in the radiance data. This left 772 passes of which 38 could not be navigated properly because the mirror was moving during data acquisition. This latter problem occurs as the satellite passes northward across the equator. Depending on the season, the mirror might still have been moving when the satellite was as far north as 35°N, as the satellite operators attempted to avoid glint contamination. A total of 734 tapes were thus available for final processing, of which 701 were SSOF tapes and 33 were CRT tapes.

The basic data processing and display package used to process the WCTS was developed at the University of Miami by O. Brown, R. Evans, J. Brown, and A. Li. This package has been used by a number of researchers and forms the basis of the global CZCS processing at the NASA Goddard Space Flight Center [*Feldman et al.*, 1989].

The first step is ingestion of the raw, level 1 data. The individual passes were navigated to correct for errors in the satellite ephemeris. This process uses the world data base II coastlines to match up with clear portions of the coast and allows the manipulation of the apparent pitch, roll, yaw, and tilt of the sensor as well as the satellite time. This method can usually register images to within one pixel. After navigation, the data were then screened before further processing. This consisted of overlaying a grid of 5° latitude by 5° longitude "tiles" on the complete pass. This grid covered the entire WCTS domain from 15°N to 50°N and from 105°W to 140°W. Each tile was screened visually to determine which tiles had sufficient clear ocean pixels to warrant further processing. In addition to clear tiles, those tiles that had clear regions that were a continuation of clear areas in adjacent tiles were also flagged acceptable for further processing. This screening step was done to reduce the total processing time. Browse images were also created from the complete passes. The full swath was then trimmed by 100 pixels at either edge in order to eliminate spurious data that appear under the very large view angles present at the edges of the pass.

The voltages measured by the CZCS are converted into radiance using a calibration function for each wavelength. This has been the focus of considerable research, as the calibration system on board the satellite did not test the complete optical path of the sensor [*Gordon et al.*, 1983*b*]. A complete discussion of CZCS calibration is given by *Gordon* [1987]. As was discussed by *Gordon et al.* [1983*b*] and *Mueller* [1985], the CZCS degradation was particularly apparent in the 443 nm (channel 1) band. Initial models by *Gordon et al.* [1983*b*] used a parabolic decay function that had an inflection point at approximately orbit 24,400, which occurred in 1984. An improved model which eliminated this problem of "increasing" sensitivity after orbit 24,400 was developed by H. Gordon and embedded in the Miami software used in the WCTS processing. A further refinement of the calibration function [*R. Evans*, personal communication, 1989] indicates that the degradation of the CZCS was not a smooth process, but rather occurred as a series of discrete events and also significantly affected the other channels. Given the sensitivity of the sensor to changes in chlorophyll concentration, errors in calibration affect the quality of the chlorophyll estimates and results in a factor of 2 uncertainty in individual images [*R. Evans*, personal communication, 1989].

The raw data files were screened for cloud and land effects with a two-step process. First, a fixed threshold was used for channel 5 (750-nm band) to separate ocean pixels from land and cloud pixels. An albedo of 22 sensor counts was used as the threshold. Then non-ocean pixels were flagged and not considered for further processing. Second, as the CZCS scans from west to east, the data are occasionally corrupted as the scanner moves from bright targets to dark targets, such as from cloud to ocean. Because of the sensor design, this sometimes results in "ringing," as the sensor amplifiers recover from saturating radiance. This effect has been described by *Mueller* [1988], who also gives a method for flagging such corrupted pixels. A version of this routine was implemented that creates another image that consists of a flag identifying pixels that may be affected by this ringing. The horizontal extent of the ringing can extend anywhere from 0 to 150 pixels, depending on the viewing geometry and the albedo of the bright target. These possible corrupted pixels remain in the data set for further processing, unlike the non-ocean pixels. Ringing can also occur to the east of land under certain conditions, but very little of the WCTS domain is affected (perhaps the region in the NE Southern California Bight to the east of the Channel Islands).

The remaining ocean pixels were then used to estimate pigment concentration. The first step in this process is atmospheric correction, which has been described by *Gordon et al.* [1983*a*] in some detail. Since scattering by the atmosphere contributes 80–90% of the total satellite-sensed signal, it must be accurately estimated. The basic assumption is that the effects of Rayleigh (molecular) and Mie (particulate) scattering can be separated unambiguously and that the radiance measured in the 670 nm band originates entirely in the atmosphere (i.e., the water-leaving radiance, $L_w \approx 0$). Correction for Rayleigh scattering was based on a single-scattering model which may not be appropriate for low sun angles [*Gordon and Castaño*, 1987; *Gordon et al.*, 1988*a*]. The aerosol correction method relies on the "clear water radiance" approach to estimating the aerosol scattering contribution to the total satellite-sensed signal. That is, at low pigment concentrations, the water-leaving radiances are well known at 520, 550, and 670 nm, so that the aerosol component can be estimated for such pixels. Such information is then used to estimate a set of epsilons that describes the scattering characteristics

of the aerosol as a function of wavelength (the function at 443 nm is estimated by extrapolation from the other wavelengths). On the basis of discussions with R. Evans (University of Miami) it was decided to use a fixed set of epsilons ($\epsilon = 1.0$ for all wavelengths). This set is appropriate for marine-type aerosols such as those that dominate the west coast where the wavelength dependence of the scattering is weak. However, it should be noted that this will not produce optimal results in all locations at all times. There are situations where the atmosphere is dominated by continental-type aerosols or where there is considerable spatial variability in aerosol type, and the "standard" epsilons are not appropriate. Processing of the global CZCS data at NASA Goddard Space Flight Center (GSFC) has also assumed a constant set of epsilons for all images [*Feldman et al.*, 1989]. Recent work by *Gordon et al.* [1988*b*] attempts to estimate the set of epsilons on a pixel by pixel basis, thus eliminating the problem of spatial variation in aerosol type. This method is still under development.

After atmospheric correction, the in-water algorithms were applied to the water-leaving radiances. These algorithms are based on in situ measurements of upwelling radiance and pigment concentrations [*Clark*, 1981]. The present algorithms are based on a pair of algorithms that use the ratio of 443 nm to 550 nm and 520 nm to 550 nm, depending on whether the pigment estimate is "high" (> 1.5 mg m^{-3}) or "low" (< 1.5 mg m^{-3}).

The pigment images were then remapped to a fixed grid. Each pixel was set to be 0.01° of latitude and longitude. Thus these images do not preserve area as one moves latitudinally. Instead, the images become distorted as the east-west dimension is a function of latitude. The individual tiles were then resampled at reduced resolution to create a mosaic image which was used in the present analysis and covered the entire study area (20°–55°N, 105°–140°W). These pixels were created by averaging blocks of 7×7 pixels. If fewer than 25 pixels were cloud-free, then an average value was not formed and the reduced-resolution pixel was flagged as cloud. Only valid (i.e., ocean) pixels were used in the average.

A2. *Sources of Error in the WCTS CZCS Data*

There are several sources of error in the final CZCS data set which consists of 734 mosaics and 9114 tiles. These can be broken down roughly into processing errors and algorithm errors. Similar to the GSFC global CZCS processing [*Feldman et al.*, 1989], the purpose of the WCTS was to deliver reasonable quality data to any interested researcher; thus a balance had to be struck between in-depth, image-by-image processing and bulk, rapid delivery of a consistently processed data set.

Processing errors are those that result from operator errors in the CZCS processing stream. These include navigation errors, undetected gain errors on the sensor, and undetected sunglint in the data. First, navigation errors are generally small; for the majority of the passes, the pixel location is good to approximately 1 km. However, there are some scenes that may have been contaminated by a moving mirror and were not flagged as such. Other errors, such as improper yaw corrections, can also occur. In general, these errors can be identified as shifts in the relative location of features in the coastline. Second, the gain on the CZCS channels was improperly identified in the original level 1 data or was set incorrectly and was not detected in the initial data screening. This results in complete algorithm failure. Usually, such scenes have all ocean values set to 0 or 1. Third, the mirror was set the wrong way to avoid glint. This type of error usually looks like a "haze" of high chlorophyll values in a region where they are not expected. In general, this is a minor problem as it is a simple matter to identify and eliminate such scenes during the navigation process.

Algorithm errors result either from the assumptions made during processing or from the basic assumptions of the CZCS algorithms. These errors include incorrect cloud masking, incorrect assumptions concerning low sun angles, aerosol removal, effects of terrestrial input, contamination by case II waters, and "switching" between the low-pigment and high-pigment in-water algorithms.

As was noted by *Eckstein and Simpson* [1990], the use of a fixed threshold based on the channel 5 albedo may result in incomplete cloud and land masking. This results in part from errors in the ground processing system which results in regularly spaced scans of apparently low radiance. This problem manifests itself as a series of scan lines across clouds and land consisting of apparent pigment retrievals. Although the spacing is usually regular (every sixteenth line [*Eckstein and Simpson*, 1990]), the spacing occasionally deviates from this pattern. Also, this noise problem is present in only a fraction of the CZCS images, primarily early in the mission of Nimbus 7. The other problem in the area of cloud and land masking relates to low albedos present in images with low sun angles and large clouds. At low sun angles, radiance is so low that it is difficult to distinguish ocean from land and cloud. Also, tall clouds can cast shadows that have a radiance low enough that the fixed threshold mask assumes that the shadow area is ocean. For land areas this is easy to detect, as there are apparent pigment retrievals over known land masses; for ocean areas, there is no easy way to detect shadows. *Eckstein and Simpson* [1990] also describe a method for a variable threshold mask for CZCS data.

As noted earlier, assumptions concerning atmospheric correction are crucial in obtaining good quality pigment estimates. The first assumption is that we can separate Rayleigh and aerosol scattering into two distinct effects. *Gordon et al.* [1983*a*] state that in general this should not be a problem, but we cannot provide a quantitative assessment of the effects of a violation of this assumption. The second assumption is that a uniform set of epsilons will work for every image. This assumption is fairly robust, but it will fail under conditions of strong temporal and spatial variability in atmospheric conditions. For instance, the assumption of uniform aerosol type will not work during strong continental input (such as during Santa Ana conditions off southern California) or very clear atmospheres, as occasionally occur off British Columbia. However, for most images off the west coast, we expect that our basic assumption of uniform epsilons will work reasonably well. *Gordon et al.* [1988*b*] present a method for making aerosol corrections on a pixel by pixel basis, which may improve the processing when the method is fully developed.

The other potential source of error in the atmospheric correction process is in the Rayleigh correction. The

algorithm used in the WCTS assumes single scattering, which may be invalid at low sun angles, for which one must account for multiple Rayleigh scattering [*Gordon and Castaño*, 1987; *Gordon et al.*, 1988*a*]. If this is not done, the radiances in the blue wavelengths are lower than they should be, resulting in apparently high chlorophyll concentrations. This is most pronounced at sun/sensor angles greater than 50°. Thus, in December, measurements north of about 35° are suspect; by the same measure, data south of 50°N should be valid between the spring and fall equinoxes. The degree of this error depends in part on the type of atmosphere that is present in the scene so one cannot give a fixed sun/sensor angle cutoff for all passes. That is, the effect may be important at smaller sun/sensor angles under certain atmospheric conditions. The present global CZCS processing uses a multiple-scattering Rayleigh model [*Feldman et al.*, 1989].

The next source of error arises in the in-water algorithms. The basic assumption is that the optical properties are those of case I water [*Morel and Prieur*, 1977]; the primary determinant of variability in the optical properties is phytoplankton pigment and covarying detritus. There are several conditions that may occur that would cause this assumption to be violated. It has been suggested that areas of high wind (and hence large areas of whitecaps on the sea surface) may result in incorrect estimates of water-leaving radiance [e.g., *Tassan*, 1981]. Terrestrial input of materials can result in incorrect phytoplankton pigment estimates. In particular, the Fraser River (British Columbia), the Columbia River (Oregon), and San Francisco Bay (California) occasionally appear as regions of spurious pigment concentrations. Coccolithophore concentrations can be high, resulting in poor pigment estimates [*Balch et al.*, 1989*a*; *Gordon et al.*, 1988*b*]. However, coccolith blooms are thought to be generally rare off the west coast, compared with the Atlantic Ocean [*Balch et al.*, 1989*a*]. Pigment degradation products, such as gelbstoffe, have different optical properties than chlorophyll, resulting in poor pigment retrievals. Although gelbstoffe is generally associated with nearshore and terrigenous sources, *K. Carder* [personal communication, 1989] has measured high gelbstoffe concentrations in filaments several hundred kilometers offshore in the California Current. High pigment concentrations are often associated with high concentrations of suspended particulates, such as detritus. These particulates can strongly affect the optical properties of the water such that L_w (670 nm) $\neq 0$. The result of this latter type of error is that oceanographic features appear in the field of L_w (670 nm) radiances, which was earlier assumed to consist only of atmospheric effects. Clearly, this will result in incorrect pigment estimates. Finally, the use of a two-part in-water algorithm (for low and high pigment) can result in discontinuities in the pigment distribution. This can be observed in the histogram of pigment values [e.g., *Denman and Abbott*, 1988] or as a "speckling" on 1-km scales in the image as the algorithm switches between the high- and the low-pigment algorithms.

The final source of errors in CZCS processing is in the area of sampling, which cannot be improved either by reducing operator error or changing the fundamental algorithms. First, the CZCS responds to a weighted average of the vertical distribution of phytoplankton pigment [*Smith*, 1981; *Gordon and Clark*, 1980]. In general, this is assumed to be over the first two optical depths. However, on occasion the distribution at depth is effectively uncorrelated with the near-surface concentration so that one cannot accurately estimate integrated water column pigment from near-surface estimates [e.g., *Hayward and Venrick*, 1982]. This problem is even more severe in estimates of water column production from CZCS data [*Balch et al.*, 1989*b*]. The second problem involves subpixel-sized clouds. This may be a serious problem, particularly on the fringes of fog and cloud banks, where small clouds may not be detected. This will result in spurious pigment estimates. The third problem is in the area of data collection. The CZCS in general was turned on over U.S. coastal waters, but not every pass was collected. SSOF relied on specific requests for data for many years before they began routine collection. Also, passes were often not collected during vacation and holiday periods, and NASA would not collect data during manned missions. The sensor began to fail in spring 1984, so collections were sporadic, especially in summer, until the final shutdown of the sensor in 1986. In addition to these gaps, there are gaps due to clouds, which are by far more troublesome. As clouds and wind patterns are closely related on the west coast of the U.S., the CZCS data are biased in time and space (see *Abbott and Zion* [1987] for a description). There is no simple solution to this problem.

A3. *Summary*

Previous work with CZCS data indicates the pigment estimates are generally within a factor of 2 of simultaneous ship estimates [e.g., *Gordon et al.*, 1983*a*, 1988*b*; *Balch et al.*, 1989*b*; *Denman and Abbott*, 1988]. The degree of scatter is usually higher at high pigment levels. As the above discussion indicates, there are clearly instances when estimates from individual images are worse than this.

The purpose of providing large sets of consistently processed CZCS data to a number of investigators is twofold: to make possible both (1) the evaluation of systematic biases in the data set and (2) the extraction of the important surface pigment signal, after accounting for the systematic biases and random noise. The present paper serves as an example of both types of analysis, which are necessary to look at the seasonal and nonseasonal variability in the WCTS. Although an improved (multiple-scattering) Rayleigh model has been used in the global CZCS processing [*Feldman et al.*, 1989], questions remain concerning other possible sources of systematic errors (uniform aerosols, etc.). Even with further improvements in the algorithms, it seems likely that analyses of these CZCS data sets will continue to require the examination of systematic bias and the extraction of the signal of interest in the presence of a fairly high level of noise. In this respect, the CZCS data are no different from other satellite data (for instance, altimeter data) and other large oceanic data sets (for instance, CalCOFI or merchant ship observations). The information is there, awaiting to be revealed by the proper combination of statistics and insight.

APPENDIX B: THE PEP METHOD

The method of principal estimator patterns [*Davis*, 1977, 1978] constructs a linear combination of a set of predictors (in this case, the EOFs of the wind variables) that explains

the largest possible fraction of the variance of another set of data (in this case, the EOFs of the pigment concentration). Formally, the time series of T measurements of the wind variables (the predictor) at X spatial locations, $v(x,t)$, and the time series of T measurements of the pigment concentrations (the predictand) at Y spatial locations, $p(y,t)$, are represented by their EOFs:

$$v(x,t) = \sum_{m=1}^{X} w_m(t) W_m(x) \qquad (B1a)$$

$$p(y,t) = \sum_{n=1}^{Y} p_n(t) P_n(y) \qquad (B1b)$$

where $w_m(t), p_n(t)$ are the orthogonal EOF time series for wind and pigment concentrations and $W_m(x), P_n(y)$ are the EOF space functions. Here x and y are generalized space coordinates, i.e., they may represent 1, 2, or 3 dimensions (even a fourth, lags in time). A subset, $\hat{v}(x,t)$ of $M(\leq X)$ of the predictor variables is chosen,

$$\hat{v}(x,t) = \sum_{m=1}^{M} w_m(t) W_m(x) \qquad (B2a)$$

and used to estimate a subset of $N(\leq Y)$ pigment EOFs,

$$\hat{p}(y,t) = \sum_{n=1}^{N} p_n(t) P_n(y) \qquad (B2b)$$

A linear estimator can be formed which gives the predictand EOFs in terms of the M predictor variables,

$$\hat{p}_n(t) = \sum_{m=1}^{M} \alpha_{nm} w_m(t) \qquad (B3a)$$

where

$$\alpha_{nm} = \frac{\langle p_n w_m \rangle}{\langle w_m^2 \rangle} \qquad (B3b)$$

Temporal averaging is denoted by angle brackets. The PEPs are formed as linear combinations of the spatial patterns of the EOFs of each variable ($W_m(x)$, $P_n(y)$), resulting in a spatial function for each, related by a single time series. The goal is to maximize the amount of predictand variance explained by the PEPs, defined as

$$E = \sum_{n=1}^{N} \langle \hat{p}_n^2 \rangle \qquad (B4a)$$

subject to the constraint that the new time series, $z_n(t)$, be orthonormal, $\langle z_n(t) z_m(t) \rangle = \delta_{mn}$. The mean square predictand, E, may be written as

$$E = \sum_{k=1}^{M} \sum_{n=1}^{N} \sum_{m=1}^{M} A_{nm} \mu_{nk} \mu_{mk} \langle z_k^2 \rangle \qquad (B4b)$$

If $\sigma_n^2 = \langle w_n^2 \rangle$, α_{nm} is given above, and matrix $\mathbf{A}$ is defined by the elements

$$A_{ij} = \sum_{n=1}^{N} \alpha_{ni} \alpha_{nj} \sigma_i \sigma_j \qquad (B5a)$$

the method of Lagrange multipliers yields the eigenvalue problem

$$\sum_j A_{nj} \mu_{jm} - \lambda_m \mu_{nm} = 0 \qquad (B5b)$$

The eigenvectors, μ_{nm}, are used to form the new spatial functions,

$$W'_n(x) = \sum_{m=1}^{M} \sigma_n \mu_{nm} W_m(x) \qquad (B6a)$$

$$P'_n(y) = \sum_{m=1}^{N} \sum_{k=1}^{M} \alpha_{mk} \sigma_k \mu_{kn} P_m(y) \qquad (B6b)$$

and the time series corresponding to each pair of spatial functions,

$$z_n(t) = \sum_{m=1}^{M} \mu_{mn} \frac{w_m(t)}{\sigma_m} \qquad (B6c)$$

The time series for the original predictor and predictand can be reconstructed as

$$\hat{v}(x,t) = \sum_{m=1}^{M} w_m(t) W_m(x) = \sum_{m=1}^{M} z_m(t) W'_m(x) \qquad (B7a)$$

$$\hat{p}(y,t) = \sum_{n=1}^{N} p_n(t) P_n(y) = \sum_{m=1}^{M} z_m(t) P'_m(y) \qquad (B7b)$$

The fraction of the variance of the original predictand EOF, $p_n(t)P_n(x)$, represented by the PEPs, is referred to as the skill in predicting the variance in that EOF S_n (Table 1), calculated from

$$S_n = \frac{\langle \hat{p}_n^2 \rangle}{\langle p_n^2 \rangle} = \sum_{m=1}^{N} \frac{\alpha_{nm}^2 \sigma_m^2}{\langle p_n^2 \rangle} \qquad (B8)$$

The percent of total pigment or wind variance accounted for by the mth PEP is also reported in Table 1, calculated for pigment as

$$100 \times \frac{\lambda_m}{\sum_k^Y \langle p_k^2(t) \rangle} \qquad (B9a)$$

where the divisor is the total variance of the original pigment concentration data set, and calculated for wind as:

$$100 \times \frac{\sum_x^X W_m'^2(x)/X}{\sum_k^X \langle w_k^2(t) \rangle} \qquad (B9b)$$

The proportion of pigment variance represented by the PEPs, S_n, may not be significantly greater than that obtained from two uncorrelated sets of data. To test this, the PEP analysis is carried out for the same sets of data but displaced in time relative to each other sufficiently to assure that any correlation between the two is fortuitous. In our case, the available wind time series is longer than that of the pigment concentrations, allowing the formation of these long lags. These time series are used to estimate S_A, the artificial skill, which is the skill expected from the PEP method if the time series are uncorrelated. The ratio of the skill to artificial skill should have a chi-square distribution, which can be used to test the significance

of the amount of variance explained by the predictor, if the number of degrees of freedom is known [*Davis*, 1977]. Following *Davis* [1978], the values of the ratio S/S_A are fit to chi-square distributions with varying numbers of degrees of freedom. The best fit in our case is found for 10 degrees of freedom, and this is used to calculate the significance level in Table 1. The significance is interpreted as the probability that a random variable will explain less of the original variance than is explained by the PEP.

Acknowledgments. This work was supported by NASA Grants NAGW-869 and NAGW-1251 and by a Killam Postdoctoral Fellowship (A.C.T.). The CZCS west coast time series was supplied by NODS at JPL. The LFM winds were obtained from NCAR and tide gauge data were obtained from Jane Huyer and Bob Smith. Gene Feldman supplied the global CZCS monthly composites. We benefitted from discussions with Dudley Chelton, Tim Cowles, Bill Pearcy, and Pat Wheeler during the data analysis. Critical comments from two anonymous reviewers resulted in a stronger, longer paper.

REFERENCES

Abbott, M. R., and P. M. Zion, Satellite observations of phytoplankton variability during an upwelling event, *Cont. Shelf Res.*, *4*, 661–680, 1985.

Abbott, M. R., and P. M. Zion, Spatial and temporal variability of phytoplankton pigment off northern California during Coastal Ocean Dynamics Experiment 1, *J. Geophys. Res.*, *92*, 1745–1756, 1987.

Bakun, A., Coastal upwelling indices, west coast of North America, 1946–71, *Tech. Rep. NNFS SSRF–671*, 103 pp., Nat. Oceanic and Atmos. Admin., Seattle, Wash., 1973.

Balch, W. M., R. W. Eppley, M. R. Abbott, and F. M. H. Reid, Bias in satellite-derived pigment measurements due to coccolithophores and dinoflagellates, *J. Plankton Res.*, *11*, 575–581, 1989*a*.

Balch, W. M., M. R. Abbott, and R. W. Eppley, Remote sensing of primary production, I, A comparison of empirical and semi-empirical algorithms, *Deep Sea Res.*, *36*, 281–295, 1989*b*.

Barale, V., and R. W. Fay, Variability of the ocean surface color field in central California near-coastal waters as observed in a seasonal analysis of CZCS imagery, *J. Mar. Res.*, *44*, 291–316, 1986.

Beardsley, R. C., C. E. Dorman, C. A. Friehe, L. K. Rosenfeld, and C. D. Winant, Local atmospheric forcing during the Coastal Ocean Dynamics Experiment, 1, A description of the marine boundary layer and atmospheric conditions over a northern California upwelling region, *J. Geophys. Res.*, *92*, 1467–1488, 1987.

Botsford, L. W., Effects of environmental forcing on age-structured populations: Northern California Dungeness crab (*Cancer magister*) as an example, *Can. J. Fish. Aquat. Sci.*, *43*, 2435–2352, 1986.

Botsford, L. W., D. A. Armstrong, and J. M. Shenker, Oceanographic influences on the dynamics of commercially fished populations, in *Coastal Oceanography of Washington and Oregon*, edited by M. R. Landry and B. M. Hickey, pp. 511–565, Elsevier, New York, 1989.

Campbell, J. W., and J. E. O'Reilly, Role of satellites in estimating primary productivity on the northwest Atlantic continental shelf, *Cont. Shelf Res.*, *8*, 179–204, 1988.

Chelton, D. B., Large-scale response of the California Current to forcing by wind stress curl, *CalCOFI Rep. 23*, pp. 130–148, Calif. Coop. Oceanic Fish. Invest., Univ. of Calif., San Diego, La Jolla, 1982*a*.

Chelton, D. B., Statistical reliability and the seasonal cycle: Comments on "Bottom pressure measurements across the Antarctic Circumpolar Current and their relation to the wind," *Deep Sea Res.*, *29*, 1381–1388, 1982*b*.

Chelton, D. B., Seasonal variability of alongshore geostrophic velocity off central California, *J. Geophys. Res.*, *89*, 3473–3486, 1984.

Chelton, D. B., and R. E. Davis, Monthly mean sea level variability along the west coast of North America, *J. Phys. Oceanogr.*, *12*, 757–784, 1982.

Chelton, D. B., P. A. Bernal, and J. A. McGowan, Large-scale interannual physical and biological interaction in the California Current, *J. Mar. Res.*, *40*, 1095–1125, 1982.

Chelton, D. B., and P. M. Kosro, Central California Coastal Circulation Study CTD observations – Cruise 8501, January 1985, *Data Rep. 129, Ref. 87-05*, Coll. of Oceanogr., Oreg. State Univ., Corvallis, 1987.

Chelton, D. B., A. W. Bratkovich, R. L. Bernstein, and P. M. Kosro, Poleward flow off central California during the spring and summer of 1981 and 1984, *J. Geophys. Res.*, *93*, 10,604–10,620, 1988.

Clark, D. K., Phytoplankton algorithms for the Nimbus-7 CZCS, in *Oceanography From Space*, edited by J. F. R. Gower, pp. 227–238, Plenum, New York, 1981.

Coastal Transition Zone Group, The Coastal Transition Zone Program, *Eos Trans. AGU*, *69*, 697–707, 1988.

Cullen, J. J., and R. W. Eppley, Chlorophyll maximum layers of the southern California Bight and possible mechanisms of their formation and maintenance, *Oceanol. Acta*, *4*, 23–32, 1981.

Davis, R. E., Techniques for statistical analysis and prediction of geophysical fluid systems, *Geophys. Astrophys. Fluid Dyn.*, *8*, 245–277, 1977.

Davis, R. E., Predictability of sea level pressure anomalies over the North Pacific Ocean, *J. Phys. Oceanogr.*, *8*, 233–246, 1978.

Davis, R. E., and P. S. Bogden, Variability on the California shelf forced by local and remote winds during the Coastal Ocean Dynamics Experiment, *J. Geophys. Res.*, *94*, 4763–4784, 1989.

Denman, K. L., and M. R. Abbott, Time evolution of surface chlorophyll patterns from cross-spectrum analysis of satellite color images, *J. Geophys. Res.*, *93*, 6789–6798, 1988.

Eckstein, B. A., and J. J. Simpson, Cloud screening coastal zone color scanner images using channel 5, *Int. J. Remote Sens.*, in press, 1990.

Enfield, D. B., and J. S. Allen, On the structure and dynamics of monthly mean sea level anomalies along the Pacific coast of North and South America, *J. Phys. Oceanogr.*, *10*, 557–578, 1980.

Eppley, R. W., E. Stewart, M. R. Abbott, and U. Heyman, Estimating ocean primary production from satellite chlorophyll, Introduction to regional differences and statistics for the Southern California Bight, *J. Plankton Res.*, *7*, 57–70, 1985.

Feldman, G., N. Kuring, C. Ng, W. Esaias, C. McClain, J. Elrod, N. Maynard, D. Endres, R. Evans, J. Brown, S. Walsh, M. Carle and G. Podesta, Ocean color: Availability of the global data set, *Eos Trans. AGU*, *70*, 634–641, 1989.

Fiedler, P. C., Satellite observations of the 1982–1983 El Niño along the U.S. Pacific coast, *Science*, *224*, 1251–1254, 1984.

Fisher, J. P., and W. G. Pearcy, Studies of juvenile salmonids off northern California, Oregon, Washington and Vancouver Island, 1984, Data report, *Ref. 85-2*, Coll. of Oceanogr., Oreg. State Univ., Corvallis, 1985*a*.

Fisher, J. P., and W. G. Pearcy, Studies of juvenile salmonids off the Oregon and Washington Coast, 1985, Data report, *Ref. 85-14*, Coll. of Oceanogr., Oreg. State Univ., Corvallis, 1985*b*.

Fisher, J. P., W. G. Pearcy, and A. W. Chung, Studies of juvenile salmonids off the Oregon and Washington coast, 1983, Data report, *Ref. 84-2*, Coll. of Oceanogr., Oreg. State Univ., Corvallis, 1984.

Flament, P., L. Armi, and L. Washburn, The evolving structure of an upwelling element, *J. Geophys. Res.*, *40*, 11,765–11,778, 1985.

Freeland, H. J., W. R. Crawford, and R. E. Thomson, Currents along the Pacific coast of Canada, *Atmos. Ocean*, *22(2)*, 151–172, 1984.

Gordon, H. R., Calibration requirements and methodology for remote sensors viewing the ocean in the visible, *Remote Sens. Environ.*, *22*, 103–126, 1987.

Gordon, H. R., and D. J. Castaño, The coastal zone color scanner atmospheric correction algorithm: Multiple scattering effects, *Appl. Opt.*, *26*, 2111-2122, 1987.

Gordon, H. R., and D. K. Clark, Remote sensing optical properties of a stratified ocean: an improved interpretation, *Appl. Opt.*, *19*, 3428–3430, 1980.

Gordon, H. R., D. K. Clark, J. W. Brown, O. B. Brown, R. H.

Evans, and W. W. Broenkow, Phytoplankton pigment concentrations in the Middle Atlantic Bight: Comparison of ship determinations and CZCS estimates, *Appl. Opt.*, *22*, 20–36, 1983*a*.

Gordon, H. R., J. W. Brown, O. B. Brown, R. H. Evans, and D. K. Clark, Nimbus 7 CZCS: Reduction of its radiometric sensitivity with time, *Appl. Opt.*, *22*, 3929–3931, 1983*b*.

Gordon, H. R., J. W. Brown, and R. H. Evans, Exact Rayleigh scattering calculations for use with the Nimbus-7 coastal zone color scanner, *Appl. Opt.*, *27*, 862–871, 1988*a*.

Gordon, H. R., O. B. Brown, R. H. Evans, J. W. Brown, R. C. Smith, K. S. Baker, and D. K. Clark, A semi-analytic radiance model of ocean color, *J. Geophys. Res.*, *93*, 10,909–10,924, 1988*b*.

Haury, L. R., J. J. Simpson, J. Peláez, C. J. Koblinsky, and D. Wiesenhahn, Biological consequences of a recurrent eddy off Point Conception, California, *J. Geophys. Res.*, *91*, 12,937–12,956, 1986.

Hayward, T. L., and E. L. Venrick, Relation between surface chlorophyll, integrated chlorophyll, and integrated primary production, *Mar. Biol.*, *69*, 247–252, 1982.

Hickey, B. M., The California current system—Hypotheses and facts, *Prog. Oceanogr.*, *8*, 191–279, 1979.

Hickey, B. M., Patterns and processes of circulation over the continental shelf off Washington, in *Coastal Oceanography of Washington and Oregon*, edited by M. R. Landry and B. M. Hickey, pp. 41–115, Elsevier, New York, 1989.

Hotelling, H., Relations between two sets of variates, *Biometrika*, *28*, 321–377, 1936.

Huyer, A. E., Coastal upwelling in the California current system, *Progr. Oceanogr.*, *12*, 259–284, 1983.

Huyer, A. E., and R. L. Smith, The signature of El Niño off Oregon, 1982–1983, *J. Geophys. Res.*, *90*, 7133–7142, 1985.

Huyer, A. E., E. J. Sobey, and R. L. Smith, The spring transition in currents over the Oregon continental shelf, *J. Geophys. Res.*, *84*, 6995–7011, 1979.

Ikeda, M., and W. J. Emery, Satellite observations and modeling of meanders in the California Current system off Oregon and northern California, *J. Phys. Oceanogr.*, *14*, 1434–1450, 1984.

Kosro, P. M., and A. Huyer, CTD and velocity surveys of seaward jets off northern California, July 1981 and 1982, *J. Geophys. Res.*, *91*, 7680–7690, 1986.

Landry, M. R., J. R. Postel, W. K. Peterson, and J. Newman, Broad-scale distributional patterns of hydrographic variables on the Washington/Oregon shelf, in *Coastal Oceanography of Washington and Oregon*, edited by M. R. Landry and B. M. Hickey, pp. 1–40, Elsevier, New York, 1989.

McGowan, J. A., El Niño 1983 in the Southern California Bight, in *El Niño North*, edited by W. S. Wooster and D. L. Fluharty, pp. 166–184, Washington Sea Grant Program, University of Washington, Seattle, 1985.

Mackas, D. C., G. C. Louttit, and M. J. Austin, Spatial distribution of zooplankton and phytoplankton in British Columbia coastal waters, *Can. J. Fish. Aquatic Sci.*, *37*, 1476–1487, 1980.

Martin, J. H., and R. M. Gordon, Northeast Pacific iron distribution in relation to phytoplankton productivity, *Deep Sea Res.*, *35*, 177–196, 1988.

Michaelsen, J., X. Zhang, and R. C. Smith, Variability of pigment biomass in the California Current system as determined by satellite imagery, 2, Temporal variability, *J. Geophys. Res.*, *93*, 10,883–10,896, 1988.

Miller, C. B., H. P. Batchelder, R. D. Brodeur, and W. G. Pearcy, Response of the zooplankton and ichthyoplankton off Oregon to the El Niño event of 1983, in *El Niño North*, edited by W. S. Wooster and A. L. Fluharty, pp. 185–187, Washington Sea Grant Program, University of Washington, Seattle, 1985.

Morel, A., and L. Prieur, Analysis of variations in ocean color, *Limnol. Oceanogr.*, *22*, 709–722, 1977.

Moum, J. N., D. R. Caldwell, and P. J. Stabeno, Mixing and intrusions in a rotating cold-core feature off Cape Blanco, Oregon, *J. Phys. Oceanogr.*, *18*, 823–833, 1988.

Mueller, J. L., Numbus-7 CZCS: Confirmations of its radiometric sensitivity decay rate through 1982, *Appl. Opt.*, *24*, 1043–1047, 1985.

Mueller, J. L., Nimbus-7 CZCS: Electronic overshoot due to cloud reflectance, *Appl. Opt.*, *27*, 438–440, 1988.

Mullin, M. M., Spatial and temporal scales and patterns, in *Plankton Dynamics of the Southern California Bight*, edited by R. W. Eppley, pp. 216–273, Springer-Verlag, New York, 1986.

Nelson, C. S., Wind stress and wind stress curl over the California Current, *Rep. NMFS SSRF-714*, 87 pp., Nat. Oceanic and Atmos. Admin., Monterey, Calif., 1977.

Niiler, P. P., P.-M. Poulain, and L. R. Haury, Synoptic three-dimensional circulation in an onshore-flowing filament of the California Current, *Deep Sea Res.*, *36*, 385–405, 1989.

Norton, J., D. McLain, R. Brainard, and D. Husby, The 1982–83 El Niño event off Baja and Alta California and its ocean climate context, in *El Niño North*, edited by W. S. Wooster and D. L. Fluharty, pp. 44–72, Washington Sea Grant Program, University of Washington, Seattle, 1985.

Pan, D., J. F. R. Gower, and G. A. Barstad, Seasonal variation of the surface chlorophyll distribution along the British Columbia coast as shown by CZCS satellite imagery, *Limnol. Oceanogr.*, *33*, 227–244, 1988.

Pares-Sierra, A., and J. J. O'Brien, The seasonal and interannual variability of the California Current System: A numerical model, *J. Geophys. Res.*, *94*, 3159–3180, 1989.

Pavlova, Y. V., Seasonal variations of the California current, *Oceanology Engl. Transl.*, *6*, 806–814, 1966.

Pearcy, W. J., and A. Schoener, Changes in the marine biota coincident with the 1982–1983 El Niño in the northeastern subarctic Pacific Ocean, *J. Geophys. Res.*, *92*, 14,417–14,428, 1987.

Pearcy, W., J. Fisher, R. Brodeur, and S. Johnson, Effects of the 1983 El Niño on coastal nekton off Oregon and Washington, in *El Niño North*, edited by W. S. Wooster and D. L. Fluharty, pp. 188–204, Washington Sea Grant Program, University of Washington, Seattle, 1985.

Peláez, J., and J. A. McGowan, Phytoplankton pigment patterns in the California Current as determined by satellite, *Limnol. Oceanogr.*, *31*, 927–950, 1986.

Rienecker, M. M., and L. L. Ehret, Wind stress curl variability over the North Pacific from the Comprehensive Ocean-Atmosphere Data Set, *J. Geophys. Res.*, *93*, 5069–5077, 1988.

Rienecker, M. M., and C. N. K. Mooers, The 1982–1983 El Niño signal off northern California, *J. Geophys. Res.*, *91*, 6597–6608, 1986.

Richman, M. B., Rotation of principal components, *J. Climatol.*, *6*, 293–335, 1986.

Riley, G. A., Phytoplankton in the north central Sargasso Sea 1950–52, *Limnol. Oceanogr.*, *2*, 252–270, 1957.

Roesler, C. S., and D. B. Chelton, Zooplankton variability in the California Current, 1951–1982, *Rep. 20*, pp. 89–101, Calif. Coop. Oceanic Fish. Invest., Univ. of Calif., San Diego, La Jolla, 1987.

Scripps Institution of Oceanography, Physical, chemical and biological data report, *S.I.O. Ref. 84-18*, Univ. of Calif., San Diego, La Jolla, 1984*a*.

Scripps Institution of Oceanography, Physical, chemical and biological data report, *S.I.O. Ref. 84-23*, Univ. of Calif., San Diego, La Jolla, 1984*b*.

Scripps Institution of Oceanography, Physical, chemical and biological data report, *S.I.O. Ref. 84-25*, Univ. of Calif., San Diego, La Jolla, 1984*c*.

Scripps Institution of Oceanography, Physical, chemical and biological data report, *S.I.O. Ref. 84-30*, Univ. of Calif., San Diego, La Jolla, 1984*d*.

Simpson, J. J., El Niño-induced onshore transport in the California Current during 1982–1983, *Geophys. Res. Lett.*, *11*, 233–236, 1984.

Simpson, J. J., C. J. Koblinsky, J. Peláez, L. R. Haury, and D. Wiesenhahn, Temperature–plant pigment–optical relations in a recurrent offshore mesoscale eddy near Point Conception, California, *J. Geophys. Res.*, *91*, 12,919–12,936, 1986.

Smith, R. C., Remote sensing and the depth distribution of ocean chlorophyll, *Mar. Ecol.*, *5*, 359–361, 1981.

Smith, R. C., X. Zhang, and J. Michaelsen, Variability of pigment biomass in the California current system as determined by satellite imagery, 1, Spatial variability, *J. Geophys. Res.*, *93*, 10,863–10,882, 1988.

Spillane, M. C., D. B. Enfield, and J. S. Allen, Intraseasonal oscillations in sea level along the west coast of the Americas, *J. Phys. Oceanogr.*, *17*, 313–325, 1987.

Strub, P. T., and C. James, Evaluation of surface wind fields over the coastal ocean off western U.S., in *Coastal Ocean Prediction Systems*, Report of planning workshop held 31 October to 2 November 1989, Univ. of New Orleans, vol. II, edited by C. N. K. Mooers, JOI Rep., in press, 1990.

Strub, P. T., J. S. Allen, A. Huyer, R. L. Smith, and R. C. Beardsley, Seasonal cycles of currents, temperatures, winds, and sea level over the northeast Pacific continental shelf: 35°N to 48°N, *J. Geophys. Res.*, *92*, 1507–1526, 1987*a*.

Strub, P. T., J. S. Allen, A. Huyer, and R. L. Smith, Large-scale structure of the spring transition in the coastal ocean off western North America, *J. Geophys. Res.*, *92*, 1527–1544, 1987*b*.

Sverdrup, H. U., On conditions for the vernal blooming of phytoplankton, *J. Cons. Explor. Mer.*, *18*, 287–295, 1953.

Tassan, S., A global sensitivity analysis for the retrieval of chlorophyll concentrations from remotely sensed radiances—The influence of the wind, in *Oceanography From Space*, edited by J. F. R. Gower, pp. 371–376, Plenum, New York, 1981.

Thomas, A. C., and W. J. Emery, Winter hydrography and plankton distributions on the southern British Columbia shelf, *Can. J. Fish. Aquat. Sci.*, *43*, 1249–1258, 1986.

Thomas, A. C., and W. J. Emery, Relationships between near-surface plankton concentrations, hydrography, and satellite-measured sea surface temperature, *J. Geophys. Res.*, *93*, 15,733–15,748, 1988.

Thomas, A. C., and P. T. Strub, Interannual variability in phytoplankton pigment distribution during the spring transition along the west coast of North America, *J. Geophys. Res.*, *94*, 18,095–18,117, 1989.

Traganza, E. D., V. M. Silva, D. M. Austin, W. E. Hanson, and S. H. Bronsink, Nutrient mapping and recurrence of coastal upwelling centers by satellite remote sensing: Its implication to primary production and the sediment record, in *Coastal Upwelling: Its Sediment Record*, edited by E. Suess and J. Thiede, pp. 61–83, Plenum, New York, 1983.

M.R. Abbott, C. James, P.T. Strub, and A.C. Thomas, College of Oceanography, Oregon State University, Oceanography Admin. Bldg. 104, Corvallis, OR 97331.

(Received June 27, 1989;
revised November 20, 1989;
accepted November 28, 1989.